MXD4/MAD4 regulates human keratinocyte precursor fate

Julien Coutier, Frédéric Auvré, Gilles Lemaître, Jean-Jacques Lataillade, Jean-François Deleuze, Paul-Henri Roméo, Michèle T Martin, Nicolas O. Fortunel

MXD4/MAD4 Regulates Human Keratinocyte Precursor Fate

JID Open

Julien Coutier[1,2], Frédéric Auvré[1,2], Gilles Lemaître[1,2], Jean-Jacques Lataillade[3], Jean-François Deleuze[4], Paul-Henri Roméo[5,6,7], Michèle T. Martin[1,2,8] and Nicolas O. Fortunel[1,2,8]

Deciphering the pathways that regulate human epidermal precursor cell fate is necessary for future developments in skin repair and graft bioengineering. Among them, characterization of pathways regulating the keratinocyte (KC) precursor immaturity versus differentiation balance is required for improving the efficiency of KC precursor ex vivo expansion. In this study, we show that the transcription factor *MXD4*/MAD4 is expressed at a higher level in quiescent KC stem/progenitor cells located in the basal layer of human epidermis than in cycling progenitors. In holoclone KCs, stable short hairpin-RNA–mediated decreased expression of *MXD4*/MAD4 increases MYC expression, whose modulation increases the proliferation of KC precursors and maintenance of their clonogenic potential and preserves the functionality of these precursors in three-dimensional epidermis organoid generation. Altogether, these results characterize *MXD4*/MAD4 as a major piece of the stemness puzzle in the human epidermis KC lineage and pinpoint an original avenue for ex vivo expansion of human KC precursors.

Journal of Investigative Dermatology (2023) **143,** 105–114; doi:10.1016/j.jid.2022.07.020

INTRODUCTION

The fields of tissue replacement strategies and knowledge of stem cell (SC) biology are intrinsically linked. As a textbook example of this interconnection, the human epidermis is endowed with a remarkable regenerative capacity owing to the presence of a compartment of resident keratinocyte (KC) SCs. The potential of these SCs has enabled the development of skin organoids, including skin substitutes that have proved efficient for grafting in patients suffering extensive burn wounds (Gallico et al., 1984; Ronfard et al., 2000) and for gene therapy (Hirsch et al., 2017). Of note, successful long-term graft outcome relies on the presence of functional KC SCs within grafts, whose preservation during the massive ex vivo cellular expansion required for the bioengineering of large surfaces of skin substitutes thus represents a major issue (up to one square meter of bioengineered graft produced from few square centimeters of skin biopsies).

KC SCs have been functionally defined as holoclones (Barrandon and Green, 1987). Holoclones have been extensively characterized at the functional level and for their clinical relevance. These cells possess an extensive proliferative capacity exceeding 100 population doublings (PDs), associated with an efficient potential for three-dimensional epidermis organoid reconstruction (Fortunel et al., 2010). Of note, a link between holoclones and epidermis regeneration prognosis in the treatment of massive full-thickness skin burns by cultured epithelial substitute grating has been reported (Ronfard et al., 2000) as well as their relevance as target cells for long-term gene therapy (Droz-Georget Lathion et al., 2015). Notably, the efficient regeneration and genetic correction of the entire epidermis of a child suffering from junctional epidermolysis bullosa has been attributed to the regenerative potential of holoclones (Hirsch et al., 2017). Holoclones also ensure a central function in replacement strategies concerning the cornea (Rama et al., 2010).

Although the importance of preserving the potential associated with holoclones in an ex vivo environment is strongly established, deciphering the signaling networks that ensure the controls of stemness and self-renewal in this cellular model is still an open research area. In this context, previous work carried out by our group identified the Krüppel-like factor 4 transcription factor as a regulator of stemness in the human KC lineage, in relation to the TGFB regulation network, and documented its use as a target to improve their ex vivo amplification and regenerative capacity (Fortunel et al., 2019). In this line, this study investigates the influence of the candidate gene *MXD4*, which encodes the MAX-interacting transcriptional repressor MAD4 (Hurlin et al., 1996), on holoclone KC expansion.

Previous studies pointed out the role of MAD4 in development and in SCs. During rodent embryogenesis, upregulation of *MAD* family genes, including *MXD4*, is associated with the downregulation of *MYC* in the developing CNS and epidermis (Hurlin et al., 1996). During in vitro hematopoiesis of murine

[1]*Laboratory of Genomic and Radiobiology of Keratinopoiesis, CEA/DRF/IBFJ/IRCM, Evry, France;* [2]*Paris-Saclay University, Evry Val-d'Essonne University, Evry, France;* [3]*INSERM UMRS-MD 1197, Institute of Armies Biomedical Research (IRBA), Armies Blood Transfusion Centre, Clamart, France;* [4]*National Centre of Human Genomic Research, CEA/DRF/IBFJ, Evry, France;* [5]*CEA-INSERM UMR1274, Research Laboratory on Repair and Transcription in hematopoietic Stem Cells, CEA/DRF/IBFJ/IRCM, Fontenay-aux-Roses, France;* [6]*Paris-Diderot University, Paris, France; and* [7]*Paris-Saclay University, Gif-sur-Yvette, France*

[8]*These authors contributed equally to this work.*

Correspondence: Nicolas O. Fortunel, DRF - JACOB/IRCM/LGRK, Alternatives Energies and Atomic Energy Commission (CEA), 2 Rue Gaston Crémieux, Evry 91057 CEDEX, France. E-mail: nicolas.fortunel@cea.fr

Abbreviations: KC, keratinocyte; KD, knockdown; PD, population doubling; RNA-seq, RNA sequencing; SC, stem cell; shRNA, short hairpin-RNA; WT, wild-type

Received 12 December 2021; revised 30 June 2022; accepted 13 July 2022; accepted manuscript published online 22 August 2022

embryonic SCs, *MXD4*/MAD4 regulates blood precursor proliferation, and its decreased expression may be required for a proliferative burst preceding lineage specification (Boros et al., 2011). Finally, overexpression of *MXD4*/MAD4 in human adipose–derived SCs inhibits adipogenesis in vitro (Li et al., 2019).

This study shows that maintaining *MXD4*/MAD4 expression at a low level increased the in vitro immaturity, growth, and clonogenic potential of KC precursor cells and promoted the maintenance of their potential for the reconstruction of three-dimensional epidermis organoids.

RESULTS AND DISCUSSION

MXD4 is expressed at a high level in quiescent epidermal SCs and regulates the MYC/MAX/MAD4 equilibrium

Comparative transcriptome microarray profiling of human primary basal KC subpopulations enriched in SCs (ITGA6^{bright} / TFR1^{dim}) or in progenitors (ITGA6^{bright} / TFR1^{bright}) (Li et al., 1998; Rachidi et al., 2007) (complete datasets are available in the Gene Expression Omnibus database, accession number GSE68583) shows that *MXD4* was expressed in the two subpopulations and that its mRNA level was 6.6-fold higher in quiescent SCs than in cycling progenitors (Supplementary Table S1). RT-qPCR validated this *MXD4* mRNA higher level (Supplementary Figure S1a). In accordance, MAD4 protein was colocalized with ITGA6^{+} KCs and was mostly detected in the basal layer of the epidermis (Supplementary Figure S1b–e) that contains the KC stem and progenitor cells.

Protein–protein interactions between MAD4, MAX, and MYC transcription factors regulate transcription. MAX proteins are ubiquitous and can form either homodimers that do not regulate transcription or MYC/MAX and MAD/MAX heterodimers, which respectively activate and repress the transcription of target genes (Ayer et al., 1993; Blackwood et al., 1992; Kato et al., 1992). MYC/MAX increases proliferation, whereas MAD4/MAX represses proliferation and induces differentiation (Rottmann and Luscher, 2006). To study this cross-talk in human immature KC precursors, samples of holoclone KCs were transduced with a lentiviral vector designed for short hairpin-RNA (shRNA)-mediated *MXD4* knockdown (KD) and GFP expression and sorted according to GFP expression. *MXD4*^{KD} cells displayed significant repression of *MXD4*/MAD4 expression at mRNA and protein levels (Supplementary Figure S2a–d). As a control, nontransduced cells and cells transduced with vectors containing either *GFP* alone or *GFP* and anti-*Luc* shRNA (*MXD4* wild-type [WT]) exhibited similar properties (Fortunel et al., 2019). Of note, shRNA-mediated *MXD4* repression was stable because it abolished the progressive increase of *MXD4* level that occurred during expansion (Supplementary Figure S3). The specificity of the cellular responses promoted by *MXD4* repression was documented by the use of two shRNA sequences for stable KD experiments and the use of two small interfering RNA sequences for transient KD experiments (Supplementary Table S2).

Expression of the *MYC*, *MAX*, and *MAD4* factors was studied at mRNA and protein levels in *MXD4*^{WT} and *MXD4*^{KD} cells. MAX was expressed at similar levels in the two cellular contexts, whereas MYC expression level was increased in *MXD4*^{KD} cells (Figure 1a–c). These results show that decreased expression of MAD4 is associated with increased expression of MYC and thus modifies the equilibrium between MAD4/MAX and MYC/MAX dimers, favoring the latter ones. This modified balance between MAD4/MAX and MYC/MAX dimers might drive mitogenic signals (Supplementary Figure S4), in addition to the previously reported impact on KC differentiation (Watt et al., 2008).

MXD4/MAD4 expression level regulates the proliferation of epidermal KC precursor cells

To characterize the functional consequences of *MXD4* KD, we used human holoclone KCs because these cells possess a high growth potential associated with the long-term capacity for epidermal regeneration, providing an ex vivo model of immature KC precursor fate (Fortunel et al., 2019, 2010).

Analyses of RNA-seq (RNA sequencing) (datasets in the Gene Expression Omnibus database, accession number GSE202700) of stably transduced *MXD4*^{WT} and *MXD4*^{KD} cells showed increased mRNA levels of cell-cycle activator genes in the latter, together with a decreased mRNA levels of cell-cycle inhibitor genes (Figure 2a and Supplementary Table S3). Of note, functional annotation performed using the Enrichr web server (https://maayanlab.cloud/Enrichr/) (Kuleshov et al., 2016) with an interrogation of three databases (Molecular Signatures Database Hallmark 2020, BioPlanet 2019, and Gene Ontology Biological Process 2021) specifically identified c-MYC– and E2F-related pathway regulatory elements, in addition to cell-cycle checkpoints and various regulators of cell-cycle–related functions (Supplementary Figure S5a–c). Of note, a pool of validated c-MYC effectors regulated in our model pointed out cell cycle regulation (Supplementary Figure S5d and Supplementary Table S4).

According to these data, we explored the impact of the *MXD4*^{KD} cellular context on cell-cycling activity in holoclone KCs. *MXD4*/MAD4 stable repression increased KC precursor proliferation 48 hours after plating because the number of growing colonies corresponding to ≥2 cell divisions increased from 16.1 ± 1.3 and 29.9 ± 2.3 for *MXD4*^{WT} and *MXD4*^{KD} cells, respectively (Figure 2b). In accordance, the mRNA level of the *Ki-67* proliferation marker (Figure 2c) and the percentage of cells expressing Ki-67 protein (Figure 2d) increased in *MXD4*^{KD} cells. Of note, *MXD4* repression and its consequent short-term induction of proliferation were reproduced with a second shRNA construct (Supplementary Figure S2e–g). Altogether, these results showed that the regulation of *MXD4* transcript is involved in the proliferation process of KCs.

An antagonistic action of MAD4 on MYC-dependent mitogenic signal has been documented in human fibroblast models, in which the expression of *MXD4*/MAD4 inhibited proliferation and colony formation and promoted cell-cycle arrest associated with replicative senescence (Marcotte et al., 2003). Our results thus identify an original facet of the regulatory functions of the MYC/MAX/MAD4 molecular balance, which is the control of cell cycling in KC precursors from adult human interfollicular epidermis. This finding points on *MXD4*/MAD4 as a potential target for promoting the mitogenic response of KC precursors in culture conditions.

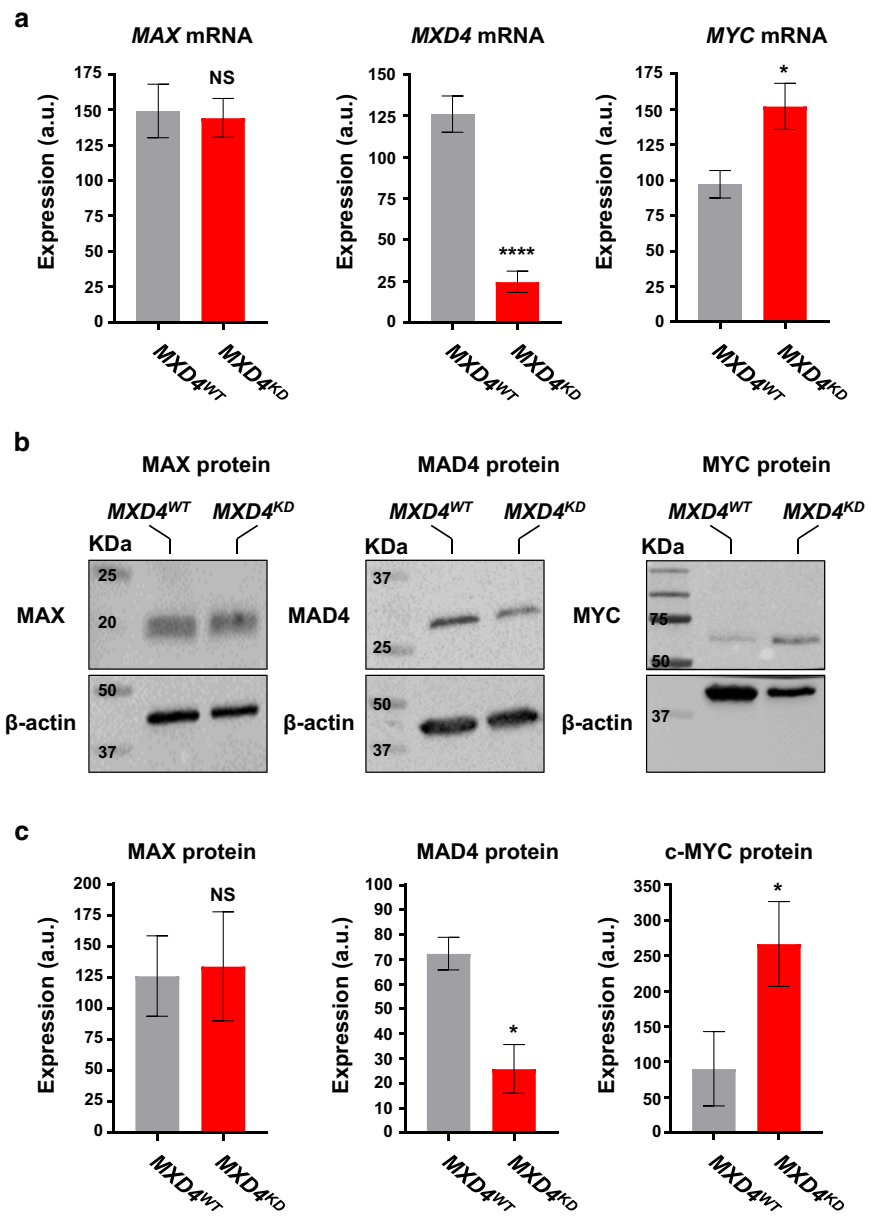

Figure 1. Modification of the MYC/MAX/MAD4 equilibrium in *MXD4*^{KD} cells. The expression level of the MYC, MAX, and MAD4 factors was analyzed at the mRNA and protein levels in *MXD4*^{WT} and *MXD4*^{KD} holoclone keratinocytes 5 weeks after transduction. (**a**) RT-qPCR analysis of *MYC*, *MAX*, and *MXD4* transcript levels in *MXD4*^{WT} and *MXD4*^{KD} cells. Signals were normalized versus *18S* transcript signal (mean ± SEM, *MAX* $P = 0.99$, n = 11; *MXD4* $P = 0.0001$, n = 8; *MYC* $P = 0.0284$, n = 20 biologically independent samples, Mann–Whitney two-sided *U* test). (**b, c**) Western blot analysis of MYC, MAD4, and MAD4 protein levels in *MXD4*^{WT} and *MXD4*^{KD} cells. (**b**) Gel pictures with β-actin detection as a loading control. Raw western blot pictures are shown in Supplementary Figure S10. (**c**) Quantification of the signals (mean ± SEM, MAX $P = 0.99$, n = 6; MAD4 $P = 0.0317$, n = 5; MYC $P = 0.0104$, n = 8 biologically independent samples, Mann–Whitney two-sided *U* test). $^*P < 0.05$, $^{****}P < 0.0001$. a.u., arbitrary unit; KD, knockdown; WT, wild-type.

Decreased expression of *MXD4*/MAD4 increases ex vivo expansion of immature epidermal precursors

We then studied the association between the mitogenic stimulation induced by the decreased expression of *MXD4*/MAD4 and immature KC precursor expansion. The growth rate of *MXD4*^{WT} and *MXD4*^{KD} was quantified for 26 days of mass culture (Figure 3a). Cell expansion rates obtained with *MXD4*^{KD} KCs were significantly higher than those obtained with *MXD4*^{KD} KCs, reaching 19.1 ± 1.0 PDs for cultures of *MXD4*^{KD} cells versus 11.8 ± 1.1 PD for cultures of *MXD4*^{WT} cells after 26 days. As for short-term induction of proliferation, the increased cell expansion obtained with *MXD4*^{KD} KCs was reproduced with a second shRNA construct (Supplementary Figure S2f–g). In contrast, stable overexpression of the full-length *MXD4* cDNA (*MXD4*^{OE}) had the expected opposite effect because it resulted in a marked decrease in KC expansion (Supplementary Figure S6a and b).

To assess any genetic deleterious effect of modulating the MYC/MAX/MAD4 balance, we performed whole-exome sequencing and DNA variant analysis in *MXD4*^{WT} and *MXD4*^{KD} cells after seven successive subcultures (Supplementary Figure S7a–d). Nearly identical variant profiles (Supplementary Figure S7a and b) were found in *MXD4*^{WT} and *MXD4*^{KD} cells. In accordance, the variant analysis focused on a selection of genes involved in the pathogenesis of squamous cell carcinoma (Supplementary Figure S7c) and basal cell carcinoma (Supplementary Figure S7d) revealed identical variant profiles, suggesting that *MXD4*/MAD4 KD did not increase de novo DNA mutations, a requirement for potential safety issues.

Because clone-forming efficiency is a functional criterion for immature precursor cells, the growth of *MXD4*^{WT} and *MXD4*^{KD} KCs was studied at a single-cell level after 4 weeks of expansion in mass culture. For each cellular context, a

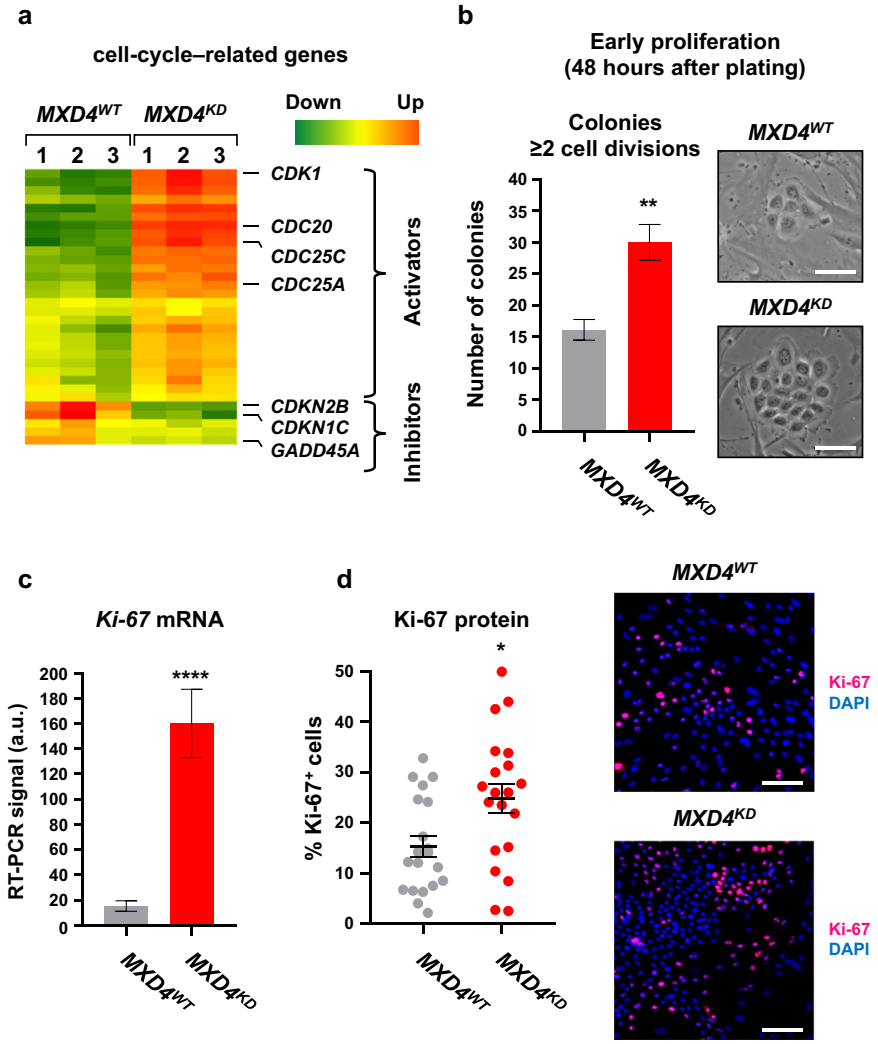

Figure 2. *MXD4*/MAD4 expression level drives epidermal precursor proliferation. Holoclone keratinocytes were transduced with lentiviral vectors driving GFP expression or expression of GFP plus a specific anti-*MXD4* shRNA, corresponding to $MXD4^{WT}$ and $MXD4^{KD}$ cellular contexts, and sorted according to GFP expression 3 days later. (**a**) Differentially expressed cell-cycle–related transcripts, identified by RNA-seq performed 5 weeks after transduction. The heatmaps shown visualize separately the gene expression levels detected in three biologically independent samples for $MXD4^{WT}$ and $MXD4^{KD}$ cells (see Supplementary Table S3, genes are in the same order). (**b**) Effect of *MXD4* KD on early cell proliferation. Growing colonies were observed 48 hours after plating, and those corresponding to ≥2 cell divisions were counted. The histogram represents the numbers of colonies obtained/25 cm^2 surface (mean ± SEM, $P = 0.0043$, n = 6 biologically independent cultures, Mann–Whitney two-sided *U* test). The photographs show representative colonies. Bars = 50 μm. (**c**) RT-qPCR analysis of *Ki-67* transcript level in $MXD4^{WT}$ and $MXD4^{KD}$ cells. Signals were normalized versus *18S* transcript level (mean ± SEM, $P = 0.0001$, n = 9 biologically independent samples, Mann–Whitney two-sided *U* test). (**d**) Percentages of cells positive for Ki-67 protein expression determined by immunofluorescence staining and high-content image analysis. Dots correspond to analyses of replicates (mean ± SEM, $P = 0.0211$, n = 20 biologically independent cultures, 2,000 cells analyzed per culture, Mann–Whitney two-sided *U* test). Typical fluorescence images are shown (Ki-67 detection and nuclei staining with DAPI). Bars = 80 μm. $*P < 0.05$, $**P < 0.01$, $****P < 0.0001$. a.u., arbitrary unit; KD, knockdown; RNA-seq, RNA sequencing; shRNA, short hairpin-RNA; WT, wild-type.

total of 1,260 cells were individually plated in parallel clonal microcultures (Fortunel et al., 2010), and their clonogenic capacity was analyzed (Figure 3b). The $MXD4^{KD}$ cell cohort produced 100 clones, whereas the $MXD4^{WT}$ cell cohort produced 24 clones. Of interest, this increase in the $MXD4^{KD}$ cell cohort was even higher when clones containing more than 2×10^4 KCs were counted (25 vs. 6 clones), indicating an increased number of immature KC precursors in the $MXD4^{KD}$ cellular context. Finally, an increased cell-surface expression of ITGA6 (data reproduced with two shRNA constructs) (Figure 3c and Supplementary Figure S2h) together with a higher expression of TP63 (ΔNp63α) were found in $MXD4^{KD}$ cells (Figure 3e), strengthening their immature phenotype. Accordingly, comparative analysis of the RNA-seq profiles of $MXD4^{WT}$ and $MXD4^{KD}$ KCs identified upregulation of transcripts associated with an immature state of basal KCs in $MXD4^{KD}$ cells and a downregulation of transcripts associated with KC differentiation (Figure 3d and Supplementary Tables S5 and S6). Interestingly, the list of upregulated transcripts is in accordance with a transcriptome signature associated with holoclones (Enzo et al., 2021), including *FOXM1*, a regulator of epidermal SCs (Supplementary Figure S5e). Of note, the increased proliferation and promotion of an immature status observed in stable

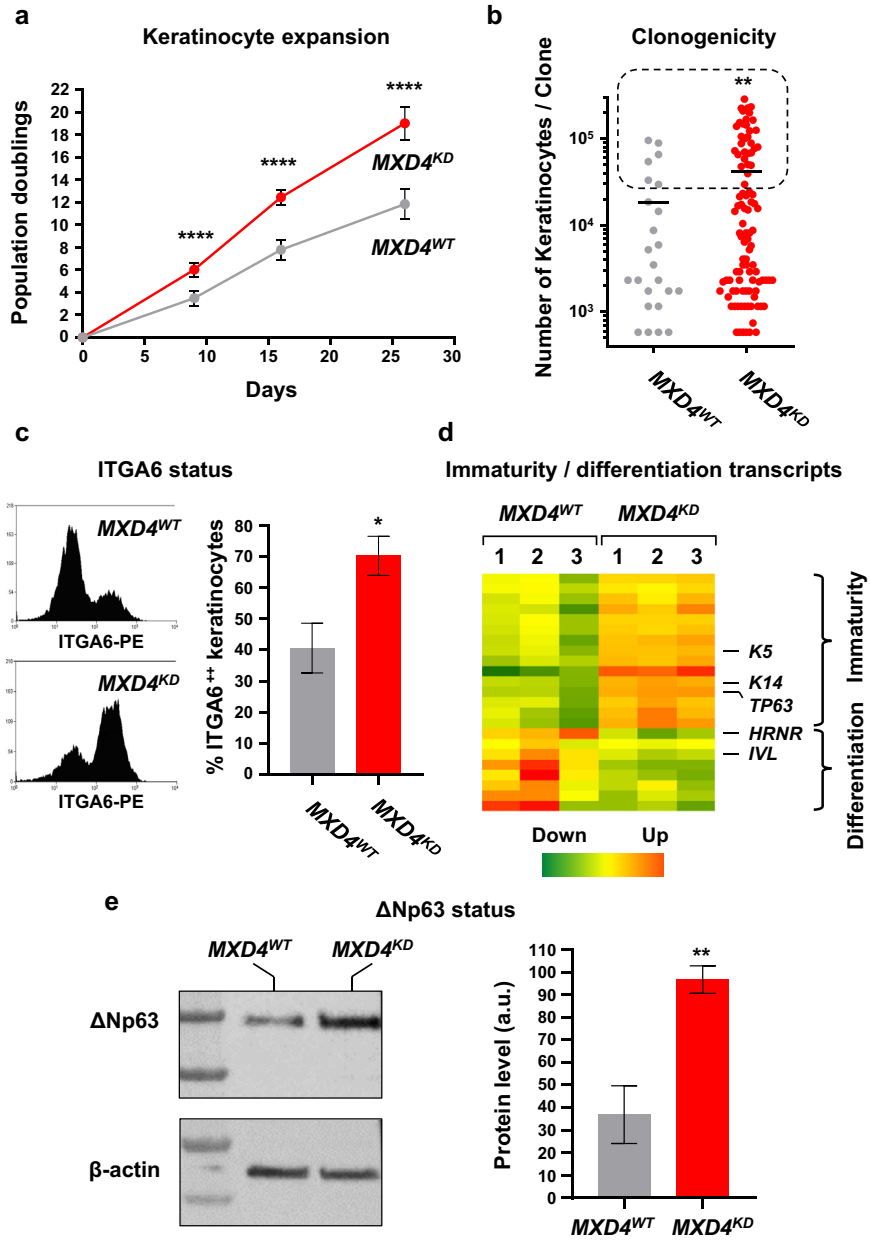

Figure 3. *MXD4* KD promotes the maintenance of an immature status. Increased growth capacity and immature characteristics of $MXD4^{KD}$ cells. (**a**) Mass cultures were performed with $MXD4^{WT}$ and with $MXD4^{KD}$ keratinocytes. Cumulative cell expansion (number of cells produced in culture/number of plated cells) was determined on days 9, 16, and 26 for the two cellular contexts ($P = 0.0001$ [day 9], $P = 0.0001$ [day 16], and $P = 0.0001$ [day 26]) (Mann–Whitney two-sided *U* test performed on 24 biologically independent samples). (**b**) Clonal growth profiles obtained with $MXD4^{WT}$ and $MXD4^{KD}$ keratinocytes amplified during 4 weeks in mass cultures, characterized in parallel clonal microcultures ($P = 0.0290$, calculated on clones with sizes ≥30,000 keratinocytes, n = 30 multiwell plates per condition, Mann–Whitney two-sided *U* test). (**c**) Analysis of ITGA6 expression by flow cytometry in $MXD4^{WT}$ and $MXD4^{KD}$ cells. Typical flow cytometry profiles are shown. Data represent the percentages of $ITGA6^{++}$ keratinocytes detected in $MXD4^{WT}$ and $MXD4^{KD}$ cells (mean ± SEM, $P = 0.0159$, n = 5 biologically independent samples, Mann–Whitney two-sided *U* test). (**d**) Heatmaps of differentially expressed transcripts associated with an immature keratinocyte precursor status 5 weeks after transduction and detected in three biologically independent samples for $MXD4^{WT}$ and $MXD4^{KD}$ cells (see Supplementary Tables S5 and S6, genes are in the same order). (**e**) Comparative analysis of ΔNp63α expression in $MXD4^{WT}$ and $MXD4^{KD}$ cells by western blotting. Typical gel photographs are shown, with β-actin detection as a loading control. Raw western blot pictures are shown in Supplementary Figure S11. Histogram of quantification (mean ± SEM, $P = 0.0087$, n = 6 biologically independent samples, Mann–Whitney two-sided *U* test). $^{*}P < 0.05$, $^{**}P < 0.01$, $^{****}P < 0.0001$. IVL, involucrin; K14, keratin 14; K5, keratin 5; KD, knockdown; PE, phycoerythrin; WT, wild-type.

shRNA-based $MXD4^{KD}$ KCs were also documented after transient *MXD4* repression by small interfering RNA transfection (Supplementary Figure S8a–d).

In summary, combined stimulation of proliferation together with improved maintenance of immaturity-associated phenotypic and functional characteristics suggested the promotion of KC precursor self-renewal that might be beneficial for the regenerative capacity of cells amplified in culture.

Decreased expression of *MXD4*/MAD4 increases epidermis organoid reconstruction capacity

Epidermis organoids were generated after 30 PD and 70 PD expansion in a two-dimensional culture of $MXD4^{WT}$ and

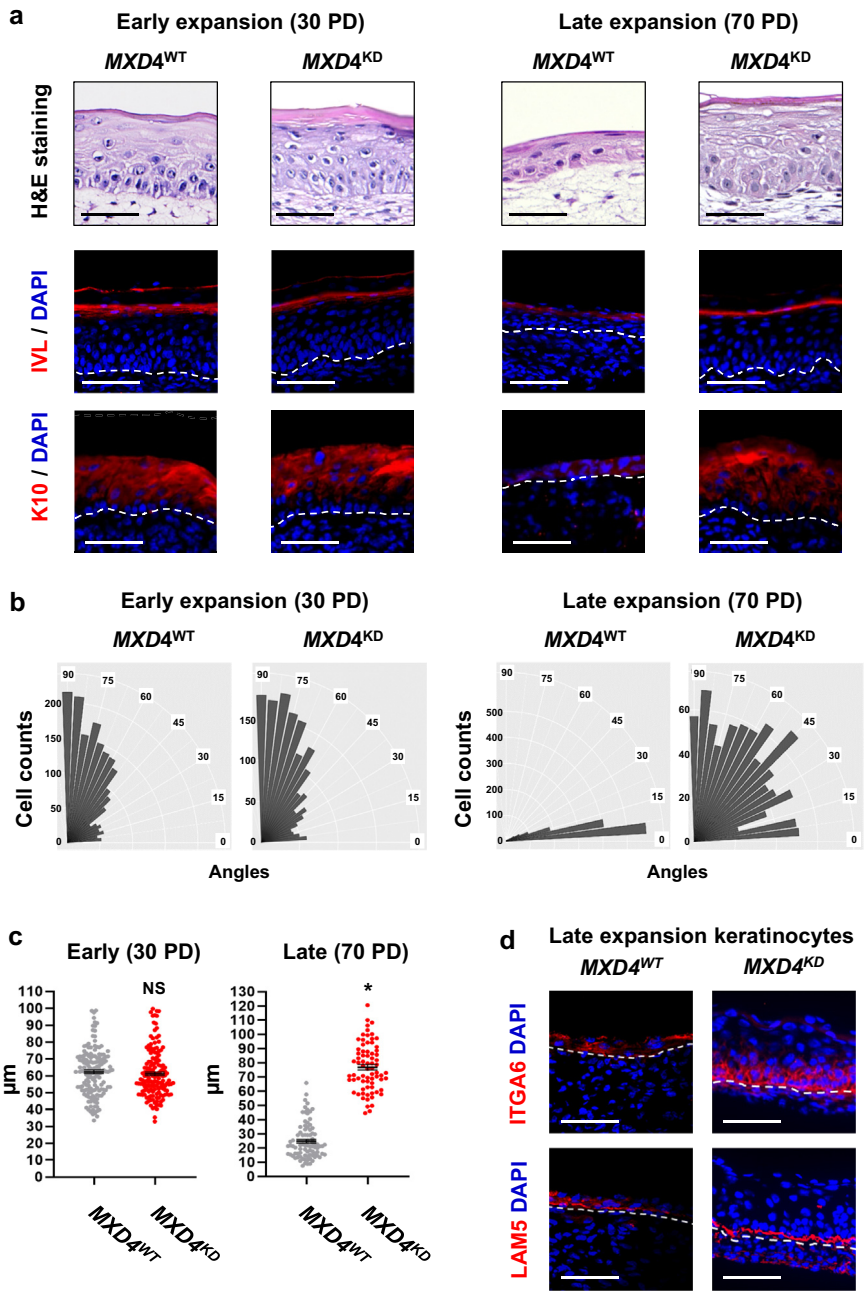

Figure 4. *MXD4* KD preserves keratinocyte epidermis reconstruction capacity. The capacity of *MXD4*^{WT} and *MXD4*^{KD} keratinocytes for in vitro three-dimensional epidermis reconstruction. (**a**) Typical histology of bioengineered epithelial sheets reconstructed on fibrin gel, obtained using *MXD4*^{WT} and *MXD4*^{KD} cells after a moderate expansion in mass culture (30 PD) and at a later stage of expansion (70 PD), associated with immunofluorescence detection of epidermal differentiation markers: IVL and K10 (n = 6 biologically independent samples per condition). Bars = 50 µm. (**b**) Basal keratinocyte nuclei orientation versus the DEJ plane was determined, after coloration with DAPI. Distribution of basal keratinocyte nuclei according to angle versus the DEJ plan into 18 angle categories from 0° to 90°, characterized by automated image analysis (graphs cumulated the analysis of nine reconstructed epidermises per condition). (**c**) Measurement of reconstructed epidermis thickness (mean ± SEM, early condition [30 PD] $P = 0.1986$, late condition [70 PD] $P = 0.0001$; n = 150 measurements performed on n = 6 biologically independent samples for each condition, Mann–Whitney two-sided *U* test). (**d**) Marker profile of reconstructed epidermises obtained with late expansion (70 PD) (*MXD4*^{WT}) and (*MXD4*^{KD}) keratinocytes: ITGA6 and LAM5 (representative immunofluorescence images from n = 6 biologically independent samples). Bars = 50 µm. *$P < 0.05$. DEJ, dermo–epidermal junction; IVL, involucrin; K10, keratin 10; KD, knockdown; PD, population doubling; WT, wild-type.

MXD4^{KD} KCs. After 30 PD expansion, the two cellular contexts generated similar differentiated pluristratified epidermises (Figure 4a, two left panels). In contrast, after 70 PD expansion, only *MXD4*^{KD} KCs could generate differentiated pluristratified epidermises (Figure 4a, two right panels). In healthy skin, basal KCs are oriented perpendicularly to the dermo–epidermal junction, and loss of this polarity is associated with alteration of epidermis integrity (Cavallero et al., 2020). Measurements of nuclei orientations versus the dermo–epidermal junction plane were performed on epidermis organoid sections by image analysis of stained nuclei (Cavallero et al., 2020). In accordance with the histology of epidermises generated by both *MXD4*^{WT} and *MXD4*^{KD} after 30 PD expansion, most nuclei were perpendicularly oriented in samples of the two contexts (Figure 4b, two left panels). This property was maintained in epidermises obtained with *MXD4*^{KD} KCs after 70 PD expansion but was lost in the epidermises produced by late-expansion *MXD4*^{WT} KCs (Figure 4b, two right panels). Reconstructed epidermis thickness (Figure 4c) together with the normal marker profile of reconstructed epidermises obtained after 70 PD expansion of *MXD4*^{KD} KCs (involucrin, keratin 10, ITGA6, and LAM5) (Figure 4a and d) further showed the functionality of these cultured *MXD4*^{KD} KC precursors.

This proper three-dimensional epidermis reconstruction with massively expanded KCs showed the maintenance of immature KC precursors carrying regenerative potential in response to *MXD4*/MAD4 decrease.

Taken together, our results identify *MXD4*/MAD4 as an important regulator of mitotic activity and immaturity versus

differentiation fate decision of human KC precursor cells amplified in culture. shRNA-mediated decreased expression of *MXD4*/MAD4 maintained an immature status, which was associated with increased preservation of KC functionality for the reconstruction of epidermis organoids. Because *MXD4*/MAD4 and TGFB1 signaling cross-talk (Siegel et al., 2003), analysis of their functional interactions should be further explored in the KC precursor model, as we recently documented for the transcription factor Krüppel-like factor 4 (Fortunel et al., 2019; Fortunel and Martin, 2020). Future development of clinically relevant prostemness agents for optimization of KC ex vivo expansion (Zhang et al., 2018) may result from the comprehension of these integrated regulatory pathways.

MATERIALS AND METHODS

Human tissue and cell materials

This study was approved by the review board of the Institut de Radiobiologie Cellulaire et Moléculaire, Commissariat à l'Energie Atomique et aux Energies Alternatives (Fontenay-aux-Roses, France) and is in accordance with the scientific, ethical, safety, and publication policy of Commissariat à l'Energie Atomique et aux Energies Alternatives (reviewed by the ethical research committee IDF-3, authorization number DC-2008-228). Human skin tissue from adult healthy donors was collected in the context of breast reduction surgery after written informed consent. Epidermal KCs and dermal fibroblasts were extracted after enzymatic treatment. Frozen banked samples of human epidermal holoclone KCs generated and characterized in the study by Fortunel et al. (2019, 2010) were studied as a model of cultured immature skin KC precursor cells.

Cell culture

Mass and clonal cultures were performed in a serum-containing medium in the presence of a feeder layer of human dermal fibroblasts growth arrested by γ irradiation (60 Gy), as described (Fortunel et al., 2019, 2010). All cultures were performed in plastic devices coated with type I collagen (Biocoat, BD, Franklin Lakes, NJ). Composition of the serum-containing medium included DMEM and Ham's F12 media (Gibco, Waltham, MA) (v/v, 3/1 mixture), 10% fetal calf serum (Hyclone Laboratories, Logan, UT), 10 ng/ml epidermal GF (Sigma-Aldrich, St. Louis, MO), 5 μg/ml transferrin (Sigma-Aldrich), 5 μg/ml insulin (Sigma-Aldrich), 0.4 μg/ml hydrocortisone (Sigma-Aldrich), 180 μM adenine (Sigma-Aldrich), 2 mM tri-iodothyronine (Sigma-Aldrich), 2 mM L-glutamine (Gibco), and 100 U/ml penicillin/streptomycin (Gibco). The medium was renewed three times a week. For mass cultures, KCs were seeded at 1,000 cells/cm^2 and subcultured every week until growth capacity was exhausted. The numbers of PDs achieved by cultures were calculated after each passage, as follows: PD = (log N/N_0)/log 2, where N_0 represents the number of plated cells, and N represents the number of cells obtained after 1 week of growth. For the clonogenicity assay, parallel clonal microcultures were initiated by automated single-cell deposition (MoFlo flow cytometer equipped with a cloning module, Beckman-Coulter, Brea, CA) in 96-well plates and exploited as described (Fortunel et al., 2010). Observation of cultures, cell counting, and analysis of early growing colonies was performed using an inverted microscope (Axio Observer D1, Carl Zeiss, Oberkochen, Germany).

High-content image analysis

Cultures of KC precursors at 50% confluence performed in 96-well plates coated with type I collagen (Biocoat, BD) were fixed with 4% paraformaldehyde for 10 minutes at 4 °C and permeabilized with PBS-Triton 0.1%. Staining was performed using nonconjugated primary antibodies, revealed using a fluorochrome-conjugated secondary antibody. Negative controls corresponded to the staining procedure without primary antibody and showed no signal (antibodies are listed in Supplementary Table S7). Nuclei were counterstained with DAPI (Fluoroshield, Sigma-Aldrich). Image acquisition and analysis were performed using a high-content imaging platform CellInsight CX7 (Thermo Fisher Scientific, Waltham, MA) equipped with the SpotDetector BioApplication.

Stable shRNA-based RNA interference

The lentiviral vector used for stable gene KD was constructed and produced by Vectalys (Vectalys, Toulouse, France). Two different shRNA vectors were designed and validated for the generation of *MXD4*/MAD4 KD (see Supplementary Table S2 for sequences and Supplementary Figure S9 for lentiviral vector characteristics). Transduction was performed on cultured holoclone KCs at 50 PDs after cloning. Transduction was performed at ∼20% confluence. Cells were incubated overnight with lentiviral particles (multiplicity of infection of 1) in the presence of hexadimethrine bromide at 8 μg/ml (Sigma-Aldrich). After 3 days, KCs at 80% confluence were collected and analyzed by flow cytometry (MoFlo, Beckman-Coulter). Transduced cells were sorted according to their GFP fluorescence.

Microarray transcriptome profiling

The transcriptional analysis that led to the identification of the candidate gene *MXD4* was based on the comparison of primary basal KC subpopulations enriched in quiescent SCs (ITGA6^{bright} / TFR1^{dim}) or in cycling progenitors (ITGA6^{bright} / TFR1^{bright}), as previously described in the study by Rachidi et al. (2007). Gene lists are available in the Gene Expression Omnibus database (www.ncbi.nlm.nih.gov/geo), accession number GSE68583.

Genome-wide transcriptome profiling by RNA-seq

The experimental design included two cellular contexts of adult KCs, each represented as three independent biological replicates: *GFP* transduced (controls) and cells transduced to express GFP and an anti-*MXD4* shRNA (*MXD4*/MAD4 KD). RNA-seq profiling of *MXD4*^{WT} and *MXD4*^{KD} KCs was performed 5 weeks after transduction. Total RNA from these six samples was extracted with RNeasy Mini and Micro kits (Qiagen, Hilden, Germany). RNA-seq libraries were then prepared according to the Illumina TruSeq protocol. The six samples were sequenced on the Illumina HiSeq 1000 as short-insert paired-end libraries with read lengths of 100 bp. The resulting 12 fastq files were processed to remove sequencing adapters and to trim low-quality bases (Phred quality score < 15) from both ends of the reads. Reads trimmed to <45 bp were discarded. Clean row read data were mapped to the *Homo sapiens* genome sequence (release GRCh38.p3) and to the associated transcriptome annotations (Ensembl release 81), downloaded from the GENCODE website. Normalization and counting were conducted using package DESeq2. Genes that had one count or less per million counts in at least two samples were filtered out as well as genes with Ensembl description qualified as empty, uncharacterized protein, or open reading frame. Sample hierarchical clustering was performed using Ward's and/or complete agglomerative method. Principal

component analysis of expression levels was performed with centered signals. The annotation-driven class discovery method was used to identify gene sets that categorized samples. Differential gene expression was assessed using the limma package (R, version 3.2.2) (datasets are in the Gene Expression Omnibus database, accession number GSE202700). Data analysis was performed with the assistance of AltraBio (Lyon, France).

Semiquantitative transcript detection by RT-qPCR

Total RNA was extracted with RNeasy Mini and Micro kits (Qiagen) followed by quality control using capillary electrophoresis (RNA 6000 Nano chips, Agilent Technologies, Santa Clara, CA). A total of 1 μg RNA was reverse transcribed using a High Capacity RNA-to-cDNA kit (Applied Biosystems, Waltham, MA). RT-qPCR reactions were carried out with gene-specific Taqman probes (Thermo Fisher Scientific) mixed with iTaq Universal Probes Supermix, according to the manufacturer's instructions (Bio-Rad Laboratories, Hercules, CA). Samples were run in triplicates in a C1000 Touch CFX96 (Bio-Rad Laboratories). Transcript expression was normalized using 18S RNA as a reference. Analysis was performed according to the ΔΔCt method (Taqman probes are listed in Supplementary Table S8).

Quantitative transcript detection by digital droplet RT-PCR

Quantitative detection of transcripts by digital droplet RT-PCR was performed as described (Auvré et al., 2019). Briefly, KC precursors processed as single-cell suspensions were used to generate samples corresponding to exactly 20 cells by flow cytometry sorting and automated deposition into wells (96-well plates) containing lysis buffer (GFP^+ cells). After cell lysis, mRNA was reverse transcribed into cDNA and mixed with TaqMan probes and digital droplet PCR Supermix for probes (Bio-Rad Laboratories). Samples were then transferred into a droplet generation cartridge, sealed, and processed for water–oil emulsion (droplet generation) using the QX200 droplet generator (Bio-Rad Laboratories). Samples were then transferred into new 96-well plates and processed for PCR using C1000 Touch thermocycler (Bio-Rad Laboratories). Quantification of the positive and negative droplets was achieved using a QX200 droplet reader (Bio-Rad Laboratories). Copy number of target sequences was determined according to the Poisson distribution, as described (Auvré et al., 2019) (TaqMan probes are listed in Supplementary Table S8).

Flow cytometry marker analyses

For analysis of ITGA6 cell-surface expression, KCs processed as single-cell suspensions were stained with phycoerythrin-conjugated rat antihuman CD49f (ITGA6) mAb (clone GoH3, BD Pharmingen, San Diego, CA). A nonreactive antibody of similar species and isotype, coupled with the same fluorochrome, was used as isotypic control. ITGA6 expression profiles were analyzed using a MoFlo cell-sorter (Beckman-Coulter) or a C6 Accuri analyzer (BD Biosciences, Franklin Lakes, NJ).

Western blot

Total proteins were extracted in RIPA buffer (Sigma-Aldrich) supplemented with antiproteases (Roche Holding, Basel, Switzerland). Protein extracts were prepared using the NE-PER kit (Thermo Fisher Scientific). Protein concentrations were determined using the micro Protein Assay Kit (BCA, Thermo Fisher Scientific). A total of 50 μg of proteins were separated by electrophoresis in Any kD Mini-PROTEAN TGX Precast Protein Gels (Bio-Rad Laboratories). Proteins were transferred onto a nitrocellulose membrane (Bio-Rad Laboratories) using the Trans-Blot SD Semi-Dry Electrophoretic Transfer Cell (Bio-Rad Laboratories). After membrane probing with primary antibodies, horseradish peroxidase–conjugated secondary antibodies (Pierce Biotechnology, Pittsburgh, PA) were used for signal detection in ECL (Clarity Western ECL, Bio-Rad Laboratories). The Chemidoc system (Bio-Rad Laboratories) was used for the detection and quantification of signals (antibodies are listed in Supplementary Table S7). Raw western blot pictures are shown in Supplementary Figures S10 and S11.

Generation of three-dimensional epidermis organoids

Model characteristics. Plasma-based human skin substitutes were reconstructed according to a procedure adapted from the study by Alexaline et al. (2015). Their characteristics were representative of a preclinical-bioengineered skin graft model. Skin reconstruction was performed in culture devices allowing two successive culture phases: immersion in the culture medium, followed by emersion at the air–liquid interphase, which provided conditions for full epidermis differentiation. Reconstructions were performed in 0.9 cm^2 culture inserts (Sigma-Aldrich), which were placed in 12 deep-well plates (Sigma-Aldrich).

Procedure. Human plasma (generous gift from Biomedical Research Institute of French Armies, INSERM U1197, Clamart, France) was mixed on ice with 4.68 mg/ml sodium chloride (Fresenius Kabi, Kriens, Swiss), 0.8 mg/ml calcium chloride (Laboratoire Renaudin, Itxassou, France), 9.7 μg/ml Exacyl (tranexamic acid, Sanofi, Paris, France), and human dermal fibroblasts. The mixture was spread in 0.9 cm^2 culture inserts, and plasma fibrin was allowed to polymerize for 30 minutes at 37 °C. Fibrin gels were then covered with a KC growth medium (the same composition as that used for two-dimensional cultures). The next day, holoclone KCs were seeded onto these dermal substrates at the density of 2,400 cells/cm^2. During the first week, cultures were maintained in the immersion phase. Wells were filled with a 5.5 ml medium (below the inserts), and a 600 μl medium was placed in the inserts, recovering the developing epidermis. During the next 2 weeks, cultures were placed in the emersion phase. Medium volume was reduced to 4 ml in wells (below the inserts), and no medium was added to the inserts to allow direct contact between the epidermis and the incubator atmosphere. Full epidermis differentiation was reached after the emersion phase.

Assessment of KC polarity in epidermis organoids

Analysis was performed on reconstructed epidermis sections stained with DAPI (Fluoroshield, Sigma-Aldrich), in which regions of interest were defined, corresponding to ~ 800 μm section length (Cavallero et al., 2020). A mask was defined by the experimenter to extract the basal KC layer and characterize nuclei orientation versus the dermo–epidermal junction plane. Angle measurements were performed automatically using a routine developed with the Fiji software, and data were plotted into 18 angle categories (from 0° to 90°) using the R software (Genethon imaging platform, Genethon, Evry, France).

Processing of reconstructed epidermis sections for immunofluorescence

Optical cutting temperature–embedded sections were thawed. Nonspecific antibody binding was blocked either by incubation in a

2% BSA solution or in serum. Staining was performed using nonconjugated primary antibodies, revealed using fluorochrome-conjugated secondary antibodies. Negative controls were performed, corresponding to the staining procedure without primary antibody, and showed no signal. Nuclei were stained with DAPI (Fluoroshield, Sigma-Aldrich). Image acquisition was performed using a Leica SP8 fluorescence imaging system. For fluorescence semiquantitative analysis, stained sections were converted into high-resolution digital slides using the Axio Scan.Z1 (Carl Zeiss) at the Genethon imaging platform (Genethon) (antibodies used for tissue section immunofluorescence analysis are listed in Supplementary Table S7).

Statistics

The statistical significance of the observed differences was determined using the Mann−Whitney two-sided *U* test.

Data availability statement

The authors declare that the main data supporting the results in this study are available within the main text and the Supplementary Materials and Methods. The raw and analyzed datasets generated during the study are available for research purposes from the corresponding authors. The transcriptome microarray and RNA-sequencing datasets that were generated have been deposited in the Gene Expression Omnibus database (www.ncbi.nlm.nih.gov/geo) and are accessible using the accession numbers GSE68583 and GSE202700, respectively.

ORCIDs

Julien Coutier: http://orcid.org/0000-0002-2407-5387
Frederic Auvré: http://orcid.org/0000-0003-3282-8163
Gilles Lemaître: http://orcid.org/0000-0002-0898-1582
Jean Jacques Lataillade: http://orcid.org/0000-0002-4594-2398
Jean-François Deleuze: http://orcid.org/0000-0002-5358-4463
Paul-Henri Roméo: http://orcid.org/0000-0002-8294-0367
Michèle T. Martin: http://orcid.org/0000-0003-0530-6466
Nicolas O. Fortunel: http://orcid.org/0000-0001-8702-247X

CONFLICT OF INTEREST

The authors state no conflict of interest.

ACKNOWLEDGMENTS

We wish to thank O. Alibert and P. Soularue for their assistance in genomic data management, L. Guibbal (Commissariat à l'Energie Atomique et aux Energies Alternatives-LGRK, Evry, France), and D. Stockholm (imaging platform, Genethon, Evry, France) for technological support. Our thanks go to H. Serhal and Y. Diaw of the Clinique de l'Essonne (Evry, France) who kindly provided human skin samples from healthy donors. Our thanks also go to Genopole (Evry, France) and notably to Julien Picot, who provided equipment and infrastructures. Our thanks also go to K. Alves, S. de Bernard, and L. Buffat from AltraBio (Lyon, France), who contributed to the analysis of RNA-sequencing data. This work was supported by grants from Commissariat à l'Energie Atomique et aux Energies Alternativesand INSERM (UMR967), Délégation Générale de l'Armement, FUI-AAP13 and the Conseil Général de l'Essonne within the STEMSAFE grant, and Electricité de France. This work also benefited from financial support provided by the Evry-val-d'Essonne, Paris-Saclay University (Evry, France). JC benefited from a Commissariat à l'Energie Atomique et aux Energies Alternatives CFR Ph.D. program fellowship and from a Ph.D fellowship from the Fondation les Gueules Cassées.

AUTHOR CONTRIBUTIONS

Conceptualization: GL, MTM, NOF; Data Curation: JC, FA, GL, MTM, NOF; Formal Analysis: JC, FA, GL, MTM, NOF; Funding Acquisition: PHR, MTM, NOF; Investigation: JC, FA, NOF; Methodology: JC, FA, JJL, MTM, NOF; Project Administration: MTM, NOF; Resources: JJL, JFD; Supervision: MTM, NOF; Validation: JJL, MTM, NOF; Visualization: JC, NOF; Writing - Original Draft Preparation: JC, NOF; Writing - Review and Editing: GL, PHR, MTM, NOF

SUPPLEMENTARY MATERIAL

Supplementary material is linked to the online version of the paper at www.jidonline.org, and at https://doi.org/10.1016/j.jid.2022.07.020

REFERENCES

Alexaline MM, Trouillas M, Nivet M, Bourreau E, Leclerc T, Duhamel P, et al. Bioengineering a human plasma-based epidermal substitute with efficient grafting capacity and high content in clonogenic cells. Stem Cells Transl Med 2015;4:643−54.

Auvré F, Coutier J, Martin MT, Fortunel NO. Quantitative detection of low-abundance transcripts at single-cell level in human epidermal keratinocytes by digital droplet reverse transcription-polymerase chain reaction. Methods Mol Biol 2019;1879:31−41.

Ayer DE, Kretzner L, Eisenman RN. Mad: a heterodimeric partner for Max that antagonizes Myc transcriptional activity. Cell 1993;72:211−22.

Barrandon Y, Green H. Three clonal types of keratinocyte with different capacities for multiplication. Proc Natl Acad Sci USA 1987;84:2302−6.

Blackwood EM, Lüscher B, Eisenman RN. Myc and Max associate in vivo. Genes Dev 1992;6:71−80.

Boros K, Lacaud G, Kouskoff V. The transcription factor Mxd4 controls the proliferation of the first blood precursors at the onset of hematopoietic development in vitro. Exp Hematol 2011;39:1090−100.

Cavallero S, Neves Granito R, Stockholm D, Azzolin P, Martin MT, Fortunel NO. Exposure of human skin organoids to low genotoxic stress can promote epithelial-to-mesenchymal transition in regenerating keratinocyte precursor cells. Cells 2020;9:1912.

Droz-Georget Lathion S, Rochat A, Knott G, Recchia A, Martinet D, Benmohammed S, et al. A single epidermal stem cell strategy for safe ex vivo gene therapy. EMBO Mol Med 2015;7:380−93.

Enzo E, Secone Seconetti A, Forcato M, Tenedini E, Polito MP, Sala I, et al. Single-keratinocyte transcriptomic analyses identify different clonal types and proliferative potential mediated by FOXM1 in human epidermal stem cells. Nat Commun 2021;12:2505.

Fortunel NO, Cadio E, Vaigot P, Chadli L, Moratille S, Bouet S, et al. Exploration of the functional hierarchy of the basal layer of human epidermis at the single-cell level using parallel clonal microcultures of keratinocytes. Exp Dermatol 2010;19:387−92.

Fortunel NO, Chadli L, Coutier J, Lemaître G, Auvré F, Domingues S, et al. KLF4 inhibition promotes the expansion of keratinocyte precursors from adult human skin and of embryonic-stem-cell-derived keratinocytes. Nat Biomed Eng 2019;3:985−97.

Fortunel NO, Martin MT. When the search for stemness genes meets the skin substitute bioengineering field: KLF4 transcription factor under the light. Cells 2020;9:2188.

Gallico GG 3rd, O'Connor NE, Compton CC, Kehinde O, Green H. Permanent coverage of large burn wounds with autologous cultured human epithelium. N Engl J Med 1984;311:448−51.

Hirsch T, Rothoeft T, Teig N, Bauer JW, Pellegrini G, De Rosa L, et al. Regeneration of the entire human epidermis using transgenic stem cells. Nature 2017;551:327−32.

Hurlin PJ, Quéva C, Koskinen PJ, Steingrímsson E, Ayer DE, Copeland NG, et al. Mad3 and Mad4: novel Max-interacting transcriptional repressors that suppress c-myc dependent transformation and are expressed during neural and epidermal differentiation. EMBO J 1996;15:2030.

Kato GJ, Lee WM, Chen LL, Dang CV. Max: functional domains and interaction with c-Myc. Genes Dev 1992;6:81−92.

Kuleshov MV, Jones MR, Rouillard AD, Fernandez NF, Duan Q, Wang Z, et al. Enrichr: a comprehensive gene set enrichment analysis web server 2016 update. Nucleic Acids Res 2016;44:W90−7.

Li A, Simmons PJ, Kaur P. Identification and isolation of candidate human keratinocyte stem cells based on cell surface phenotype. Proc Natl Acad Sci USA 1998;95:3902−7.

Li S, Xue T, He F, Liu Z, Ouyang S, Cao D, et al. A time-resolved proteomic analysis of transcription factors regulating adipogenesis of human adipose derived stem cells. Biochem Biophys Res Commun 2019;511:855−61.

Marcotte R, Qian JF, Chen J, Wang E. hMad4, c-Myc endogenous inhibitor, induces a replicative senescence-like state when overexpressed in human fibroblasts. J Cell Biochem 2003;89:576−88.

Rachidi W, Harfourche G, Lemaitre G, Amiot F, Vaigot P, Martin MT. Sensing radiosensitivity of human epidermal stem cells. Radiother Oncol 2007;83:267–76.

Rama P, Matuska S, Paganoni G, Spinelli A, De Luca M, Pellegrini G. Limbal stem-cell therapy and long-term corneal regeneration. N Engl J Med 2010;363:147–55.

Ronfard V, Rives JM, Neveux Y, Carsin H, Barrandon Y. Long-term regeneration of human epidermis on third degree burns transplanted with autologous cultured epithelium grown on a fibrin matrix. Transplantation 2000;70:1588–98.

Rottmann S, Lüscher B. The Mad side of the Max network: antagonizing the function of Myc and more. Curr Top Microbiol Immunol 2006;302:63–122.

Siegel PM, Shu W, Massagué J. Mad upregulation and Id2 repression accompany transforming growth factor (TGF)-beta-mediated epithelial cell growth suppression. J Biol Chem 2003;278:35444–50.

Watt FM, Frye M, Benitah SA. MYC in mammalian epidermis: how can an oncogene stimulate differentiation [published correction appears in Nat Rev Cancer 2008;8:316]? Nat Rev Cancer 2008;8:234–42.

Zhang C, Lee HJ, Shrivastava A, Wang R, McQuiston TJ, Challberg SS, et al. Long-term in vitro expansion of epithelial stem cells enabled by pharmacological inhibition of PAK1-ROCK-myosin II and TGF-β signaling. Cell Rep 2018;25:598–610. e5.

SUPPLEMENTARY MATERIALS AND METHODS

The methods described below are only those not described in the core manuscript.

Whole-exome sequencing

Library preparation, exome capture and sequencing, and data analysis were performed by IntegraGen SA (Evry, France). Exome capture, enrichment, and elution were performed on samples of 150 ng genomic DNA, according to the Twist Human Core Exome Enrichment System (Twist Bioscience, South San Francisco, CA). Libraries were prepared using the NEBNext Ultra II kit (New England Biolabs, Ipswich, MA). Eluted exome-enriched DNA samples were then paired-end sequenced using a HiSeq4000 (Illumina, San Diego, CA). Image analysis and base calling were performed using the Real-Time Analysis software sequence pipeline (2.7.7). Sequence reads were mapped to the Human genome build (hg38/GRCh38) using the Burrows-Wheeler Aligner tool. Variant calling, allowing identification of genetic alterations as well as Single Nucleotide Variation small insertions/deletions (up to 20 bp), was performed on the Broad Institute's GATK Haplotype Caller GVCF tool (3.7). Further variant annotation (prediction of functional consequences of variants) was performed on the Ensembl's Variant Effect Predictor program (release 92) using data available in dbSNP (dbSNP150), the gnomAD (170228), the 1000 Genomes Project (1000G_phase3), and the Exome Variant Server (NHLBI Exome Sequencing Project, V2-SSA137) and in-house databases. Genomic copy-number aberrations (copy-number gains and losses) were investigated on the Bioconductor DNACopy package (DNAcopy 1.32.0) comparing normal DNA exome data with a reference sample pool. For missense changes, two bioinformatic pathogenicity predictions were used: SIFT (sift5.2.2) and PolyPhen (2.2.2).

Stable cDNA overexpression

The lentiviral vector used for stable *MXD4* cDNA overexpression was constructed and produced by Vectalys (Vectalys, Toulouse, France) (see Supplementary Figure S11 and S12 for lentiviral vector characteristics). Transduction was performed as for short hairpin RNA lentiviral vectors (see the Materials and Methods in the core manuscript).

Transient small interfering RNA–based RNA interference

Transfection of small interfering RNAs (anti-*MXD4* or scramble) (Qiagen, Hilden, Germany) was performed on cultured keratinocytes seeded at 1,000 cells/cm^2. One day after seeding, keratinocytes were lipotransfected according to the manufacturer's instructions (Lipofectamine 3000, Thermo Fisher Scientific, Waltham, MA). Twenty-four hours after transfection, the medium was changed. Cells were harvested 5 days after transfection for numeration and flow cytometry analysis of ITGA6 cell-surface profile.

SUPPLEMENTARY REFERENCES

Bonilla X, Parmentier L, King B, Bezrukov F, Kaya G, Zoete V, et al. Genomic analysis identifies new drivers and progression pathways in skin basal cell carcinoma. Nat Genet 2016;48:398–406.

Enzo E, Secone Seconetti A, Forcato M, Tenedini E, Polito MP, Sala I, et al. Single-keratinocyte transcriptomic analyses identify different clonal types and proliferative potential mediated by FOXM1 in human epidermal stem cells. Nat Commun 2021;12:2505.

Fortunel NO, Chadli L, Coutier J, Lemaitre G, Auvre F, Domingues S, et al. KLF4 inhibition promotes the expansion of keratinocyte precursors from adult human skin and of embryonic-stem-cell-derived keratinocytes. Nat Biomed Eng 2019;3:985–97.

Kuleshov MV, Jones MR, Rouillard AD, Fernandez NF, Duan Q, Wang Z, et al. Enrichr: a comprehensive gene set enrichment analysis web server 2016 update. Nucleic Acids Res 2016;44:W90–7.

Li A, Simmons PJ, Kaur P. Identification and isolation of candidate human keratinocyte stem cells based on cell surface phenotype. Proc Natl Acad Sci USA 1998;95:3902–7.

Rachidi W, Harfourche G, Lemaitre G, Amiot F, Vaigot P, Martin MT. Sensing radiosensitivity of human epidermal stem cells. Radiother Oncol 2007;83:267–76.

Schwaederle M, Elkin SK, Tomson BN, Carter JL, Kurzrock R. Squamousness: next-generation sequencing reveals shared molecular features across squamous tumor types. Cell Cycle 2015;14:2355–61.

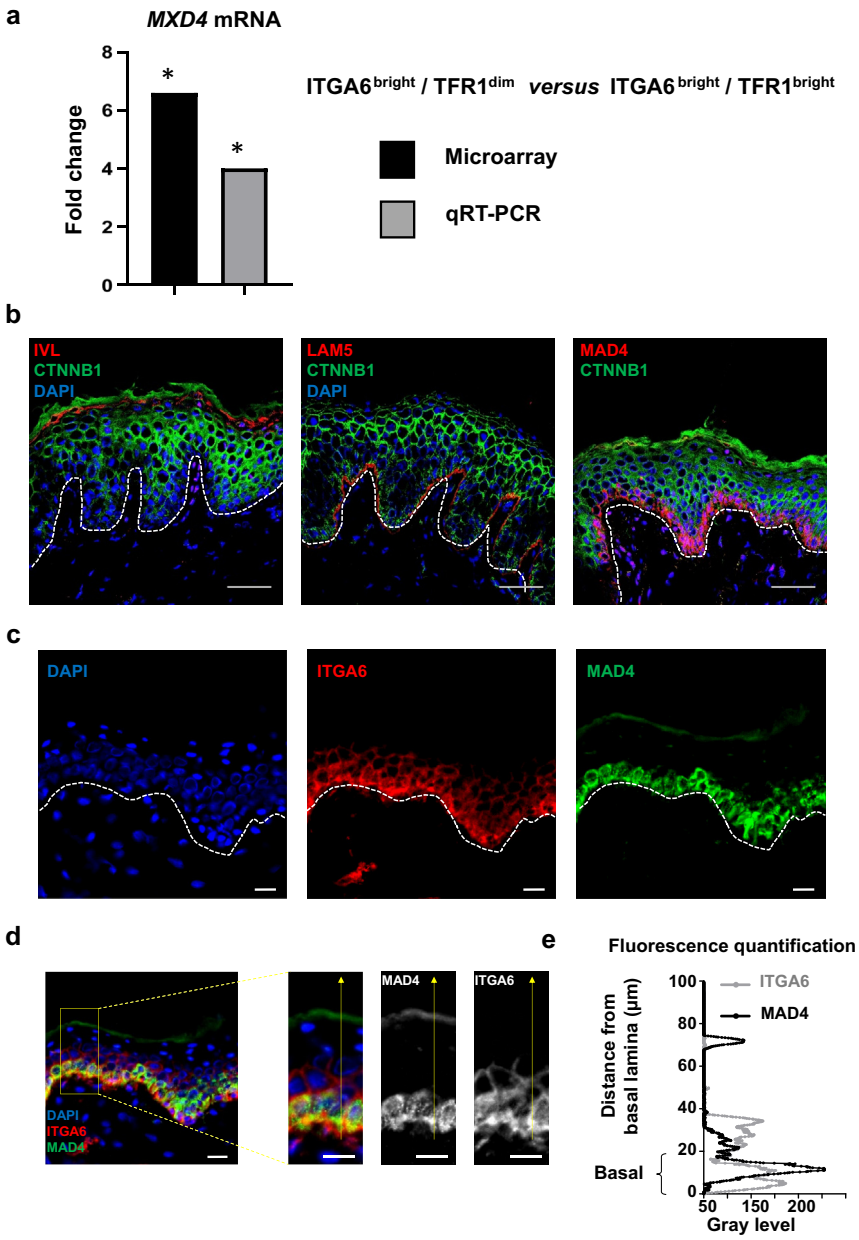

Supplementary Figure S1. *MXD4*/MAD4 identification by transcriptomic screening and predominant basal localization of MAD4 protein in the epidermis. The *MXD4*/MAD4 candidate was selected on the basis of comparative transcriptome microarray profiling of human primary basal keratinocyte subpopulations enriched in quiescent stem cells (ITGA6^{bright} / TFR1^{dim}) or in cycling progenitors (ITGA6^{bright} / TFR1^{bright}) according to the studies by Li et al. (1998), Rachidi et al. (2007), and Fortunel et al. (2019). (**a**) *MXD4* mRNA level was higher in the stem cell subpopulation than in the progenitor subpopulation (microarray and qRT-PCR validation). *$P < 0.05$. Observation of marker profiles in normal human epidermis by immunofluorescence is shown. (**b**) Suprabasal localization of IVL and β-catenin (CTNNB1) proteins and basal localization of MAD4, as visualized by the direct proximity with the basal LAM5 (nuclei stained with DAPI). Bars = 50 µm. (**c**) Colocalization of ITGA6 and MAD4. Nuclei were stained with DAPI. Bars = 25 µm. (**d, e**) Distribution of MAD4 fluorescence signal from the basal layer to the epidermis surface characterized by its colocalization with ITGA6^{+} cells. (**d**) Conversion of the fluorescence signal (arbitrary units) into gray tones (ImageJ software, National Institutes of Health, Bethesda, MD). Bars = 20 µm. (**e**) Predominant signal localization corresponding to the epidermis basal layer. Data presented in this figure were obtained using frozen sections of human neonatal foreskin. IVL, involucrin.

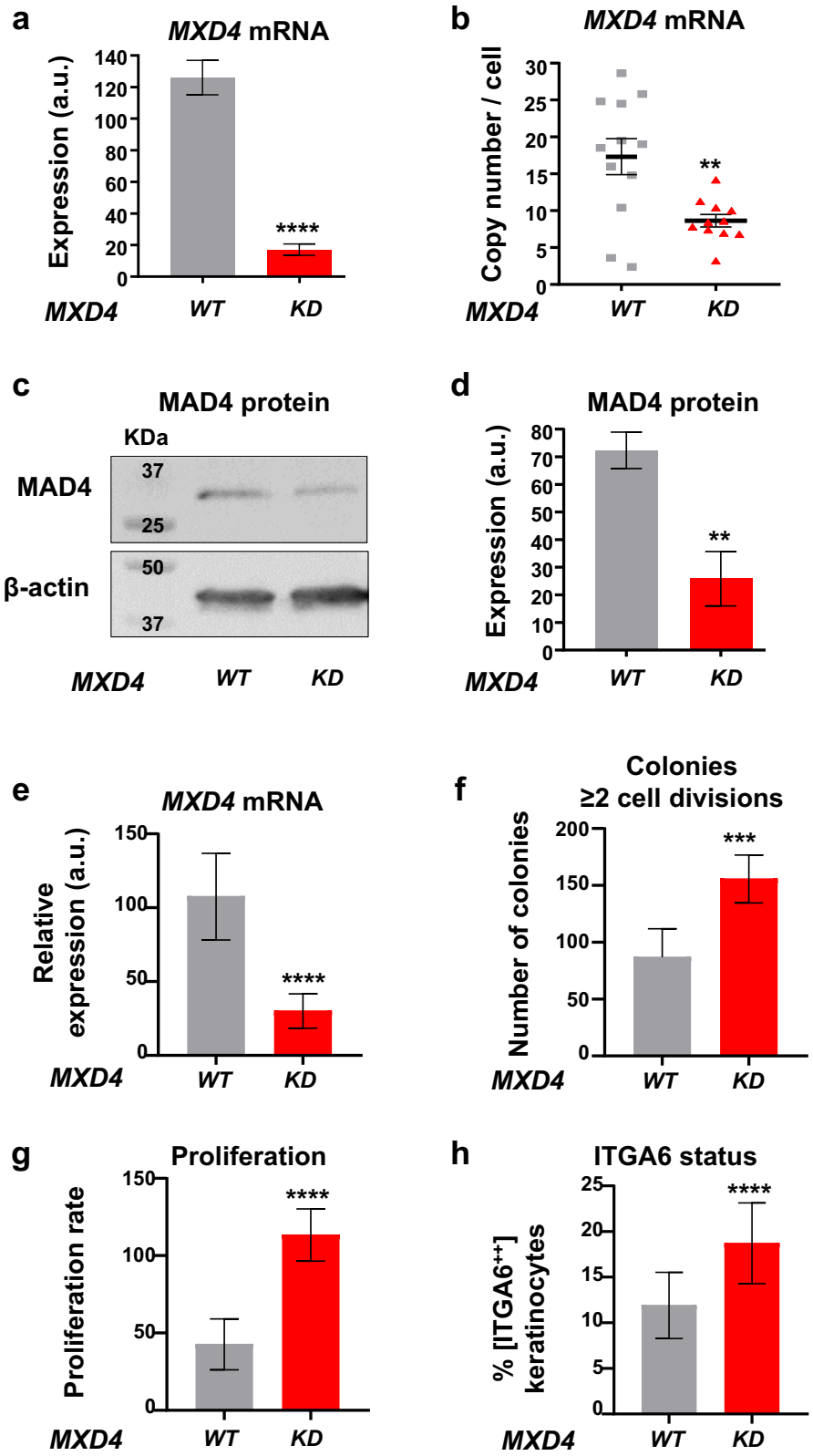

Supplementary Figure S2. Characterization of *MXD4*/MAD4 expression in the *MXD4*^{KD} cellular context using two different shRNAs. Expression of *MXD4*/MAD4 was analyzed 5 weeks after transduction (a–d) in holoclone keratinocytes transduced with a lentiviral vector designed for shRNA-mediated *MXD4* KD and GFP expression (*MXD4*^{KD}) and in holoclone keratinocytes transduced with a similar vector driving GFP expression alone (*MXD4*^{WT}). (a) shRNA-mediated downregulation of *MXD4* mRNA was documented by classical qRT-PCR (mean ± SEM, $P = 0.0001$, n = 8 biologically independent samples). The exact *P*-value was determined according to Mann–Whitney two-sided *U* test. (b) Further validation of shRNA-mediated *MXD4* mRNA downregulation by digital droplet qRT-PCR (mean ± SEM, $P = 0.0074$, n = 12 biologically independent samples). The exact *P*-value was determined according to the Mann–Whitney two-sided *U* test. (c, d) *MXD4*/MAD4 KD was also visualized at the protein level by western blotting. (c) Raw western blot and (d) estimation of MAD4 protein downmodulation level (data shown are representative from n = 5 independent experiments). (e–h) Expression of *MXD4*/MAD4 was analyzed in

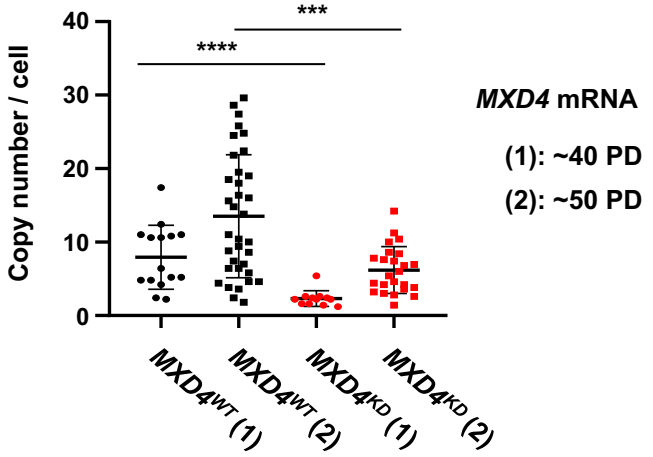

Supplementary Figure S3. Follow-up of *MXD4* mRNA level in *MXD4*^{WT} and *MXD4*^{KD} keratinocytes at ~40 and ~50 PDs by ddRT-PCR. Each reaction was performed on samples corresponding to exactly 20 cells collected by flow cytometry (n > 12 experimental replicates cumulated from n = 3 independent cultures). ddRT-PCR, digital droplet RT-PCR; KD, knockdown; PD, population doubling; WT, wild-type.

holoclone keratinocytes transduced with a second lentiviral vector designed for shRNA-mediated *MXD4* KD and GFP expression (*MXD4*^{KD}) and in holoclone keratinocytes transduced with a similar vector driving GFP expression alone (*MXD4*^{WT}). (e) Downregulation of *MXD4* mRNA induced by the second shRNA was documented by classical qRT-PCR. Signals were normalized versus 18S transcript signal (mean ± SEM, n = 12 biologically independent samples). (f) Impact of the second anti-*MXD4* shRNA on early cell proliferation. Keratinocytes were plated in six-well plates, and growing colonies were observed 96 hours after plating. Those corresponding to ≥2 cell divisions were counted. The histogram represents the numbers of colonies obtained/9.6 cm^2 surface (mean ± SEM, n = 6 biologically independent cultures). (g) Mass cultures were performed with *MXD4*^{WT} and with *MXD4*^{KD} keratinocytes obtained using the second shRNA. Cell expansion (the number of cells produced in the culture/number of plated cells) was determined on day 8 for the two cellular contexts (mean ± SEM, n = 6 biologically independent cultures). (h) Analysis of ITGA6 expression by flow cytometry in *MXD4*^{WT} and *MXD4*^{KD} cells generated with the second shRNA. Data represent the percentages of ITGA6^{++} keratinocytes detected in *MXD4*^{WT} and *MXD4*^{KD} cells (mean ± SEM, n = 6 biologically independent samples). $^{**}P < 0.01$, $^{***}P < 0.001$, $^{****}P < 0.0001$. a.u., arbitrary unit; KD, knockdown; shRNA, short hairpin RNA; WT, wild-type.

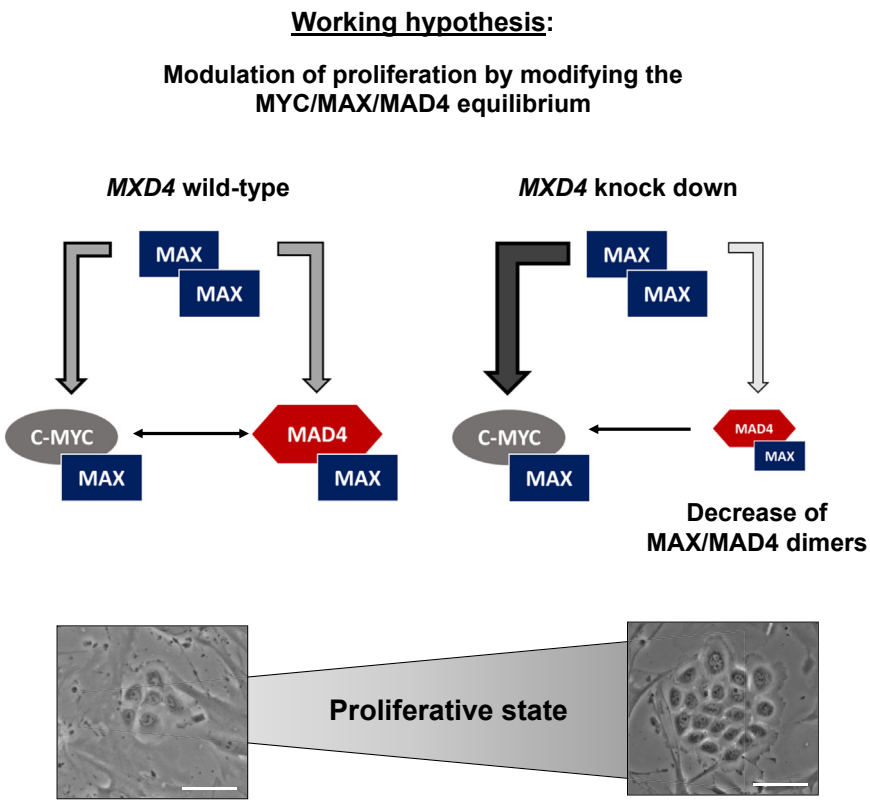

Supplementary Figure S4. Involvement of the MYC/MAX/MAD4 balance in the control of proliferation. Concomitant decrease of MAD4 and increase of MYC expression were documented in $MXD4^{KD}$ keratinocytes. Accordingly, stimulation of proliferation may result from a modification of the equilibrium between MAD4/MAX dimers and MYC/MAX dimers, favoring the latter ones and thus driving a more active mitogenic signal in $MXD4^{KD}$ cells. Bars = 50 μm.

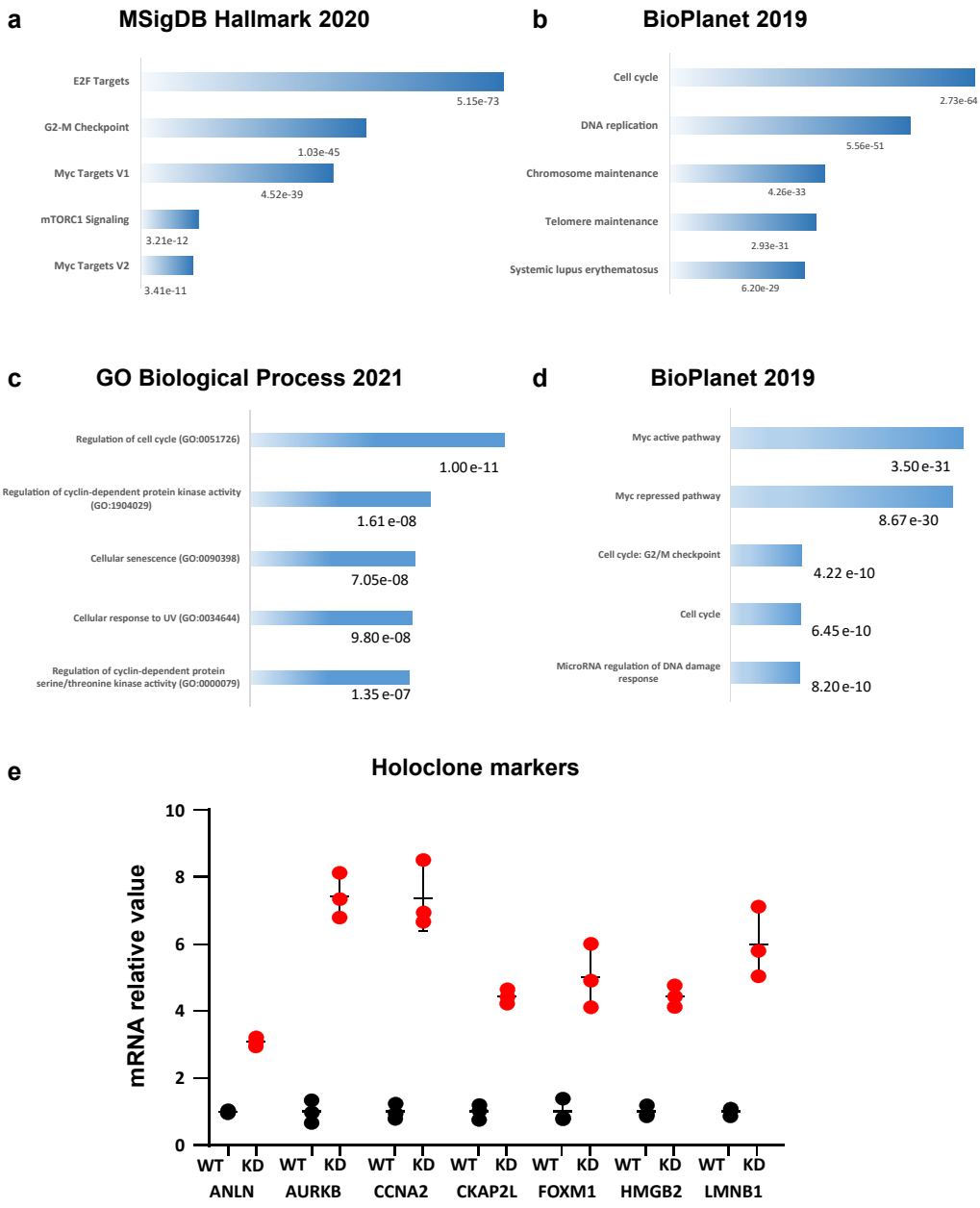

Supplementary Figure S5. Functional annotation of *MXD4*^{KD}-associated transcriptomic signatures. (**a**–**c**) Transcriptome profiles of stably transduced *MXD4*^{WT} and *MXD4*^{KD} cells characterized by RNA-seq (datasets are in the GEO database, accession number GSE202700) were functionally annotated using the Enrichr web server (https://maayanlab.cloud/Enrichr/) (Kuleshov et al., 2016) involving the interrogation of three databases (Molecular Signatures Database Hallmark 2020, BioPlanet 2019, and Gene Ontology Biological Process, 2021). Cell-cycle checkpoints and various regulators of cell-cycle–related functions were identified with a high statistical significance, in addition to MYC- and E2F-related pathway regulatory elements. (**d**) Selection of validated targets of c-Myc transcriptional repression or activation genes using PathCards (https://pathcards.genecards.org/Card/) in stably transduced *MXD4*^{WT} and *MXD4*^{KD} cells RNA-seq–deregulated genes database was annotated using Enrichr analysis. Of the 142 genes validated to be a target of MYC transcription factor, 30 were deregulated (11 upregulated and 19 downregulated) between *MXD4*^{WT} and *MXD4*^{KD} keratinocytes (Supplementary Table S6). Among these, at least 10 genes are directly related to cell cycle in BioPlanet 2019 with a *P*-value around 5E-10. (**e**) Comparative analysis of the RNA-seq profiles of *MXD4*^{WT} and *MXD4*^{KD} keratinocytes also identified increased levels of transcripts associated with an immature state of basal keratinocytes in *MXD4*^{KD} cells. For each transcript, mRNA expression in *MXD4*^{WT} and *MXD4*^{KD} keratinocytes was normalized against the mean of expression in *MXD4*^{WT}. Of note, the transcripts upregulated in this study are all found in a recently published transcriptome signature associated with holoclones (Enzo et al., 2021). GEO, Gene Expression Omnibus; GO, Gene Ontology; KD, knockdown; RNA-seq, RNA sequencing; WT, wild-type.

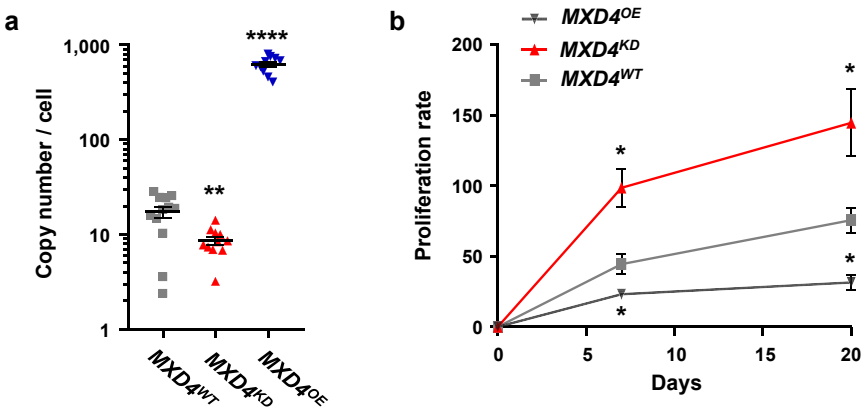

Supplementary Figure S6. Reproducibility of *MXD4*^{KD}-associated responses in *MXD4*^{OE} cells. (**a, b**) Impact of MXD4 cDNA overexpression (*MXD4*^{OE}) (see Supplementary Figure S12 for lentiviral vector characteristics). (**a**) Quantification of *MXD4* transcript level in *MXD4*^{WT}, *MXD4*^{KD}, and *MXD4*^{OE} keratinocytes by ddRT-PCR. Each reaction was performed on samples corresponding to exactly 20 cells collected by flow cytometry (n > 10 experimental replicates cumulated from n = 3 independent cultures). (**b**) Impact of *MXD4*^{OE} on keratinocyte expansion over two successive subcultures (total of 20 days) (mean ± SEM, n = 6 biologically independent samples). Stable overexpression of the full-length *MXD4* cDNA (*MXD4*^{OE}) had the opposite effect of *MXD4*^{KD} because it resulted in a marked decrease in expansion. *$P < 0.05$, **$P < 0.01$, ****$P < 0.0001$. ddRT-PCR, digital droplet RT-PCR; KD, knockdown; OE, overexpression; WT, wild-type.

Supplementary Figure S7. Absence of deleterious impact of *MXD4*^{KD} on genomic integrity. Transduced *MXD4*^{WT} and *MXD4*^{KD} were cultured for 7 weeks (seven successive subcultures) and then processed for whole-exome sequencing (Supplementary Materials and Methods) (n = 3 biologically independent samples for each cellular context). Variant profiles of *MXD4*^{WT} and *MXD4*^{KD} keratinocytes were characterized using the reference human genome hg38. Keratinocyte samples from the two cellular contexts exhibited identical variant profiles, indicating that *MXD4* downmodulation induced no genotoxic effect. (a, b) Minor differences between samples were related to technical noise or normal culture-to-culture variation. Notably, analysis of *MXD4*^{WT} and *MXD4*^{KD} cells focused on selected genes involved in keratinocyte carcinogenesis (Bonilla et al., 2016; Schwaederle et al., 2015) showed that (c) SCC gene and (d) BCC gene variant profiles were identical in the two cellular contexts. Selected SCC genes include the following: *TP53*, *KRAS* (KRAS proto-oncogene, GTPase), *CDKN2A* (encoding p16-INK4A and p14-ARF), *RB1*, *MYC* (MYC Proto-Oncogene, BHLH Transcription Factor), *KNSTRN*, *CCND1*, *NOTCH1*, *SOX2*, and *FBXW7*. Selected BCC genes include the following: *PTCH1*, *MYCN* (MYCN proto-oncogene, BHLH transcription factor), *PTPN14, PPP6C, SMO, STK19, RB1, SUFU*. BCC, basal cell carcinoma; KD, knockdown; SCC, squamous cell carcinoma.

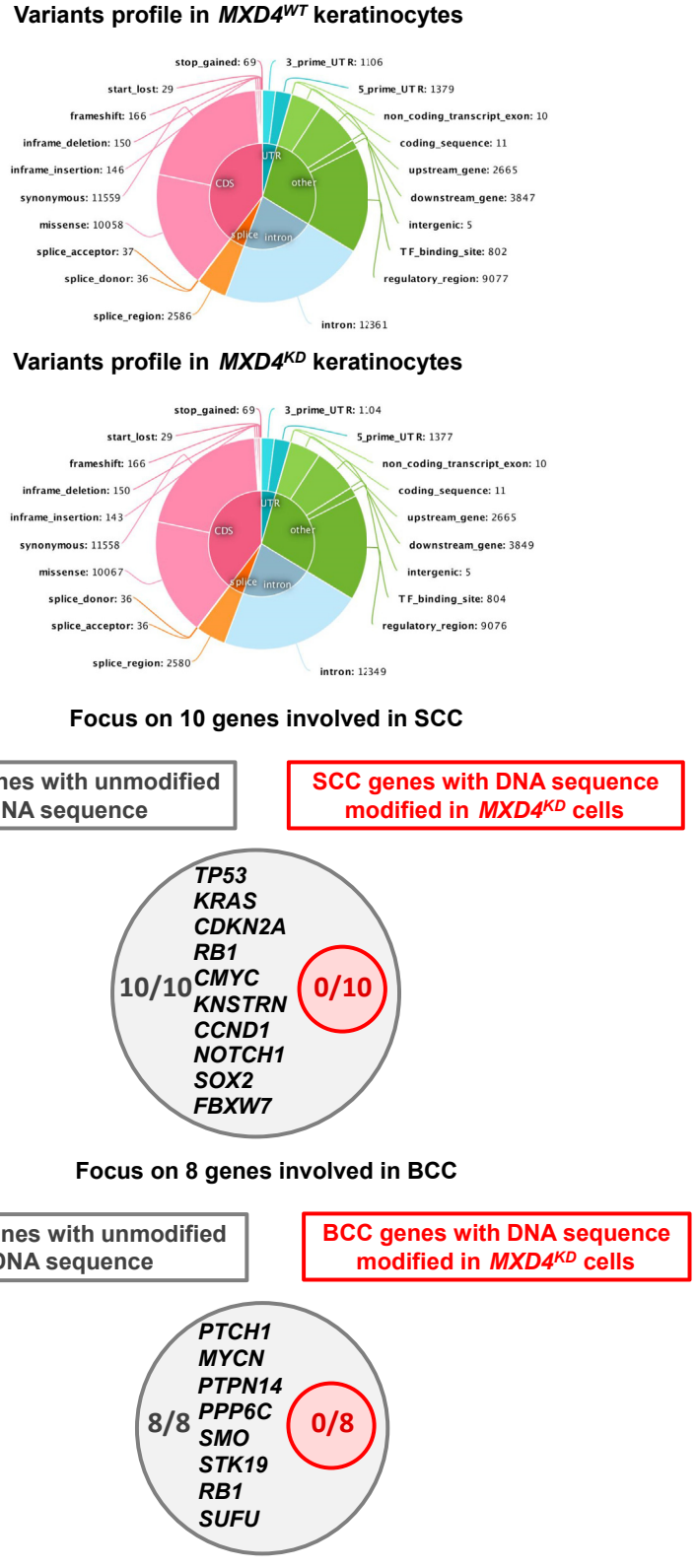

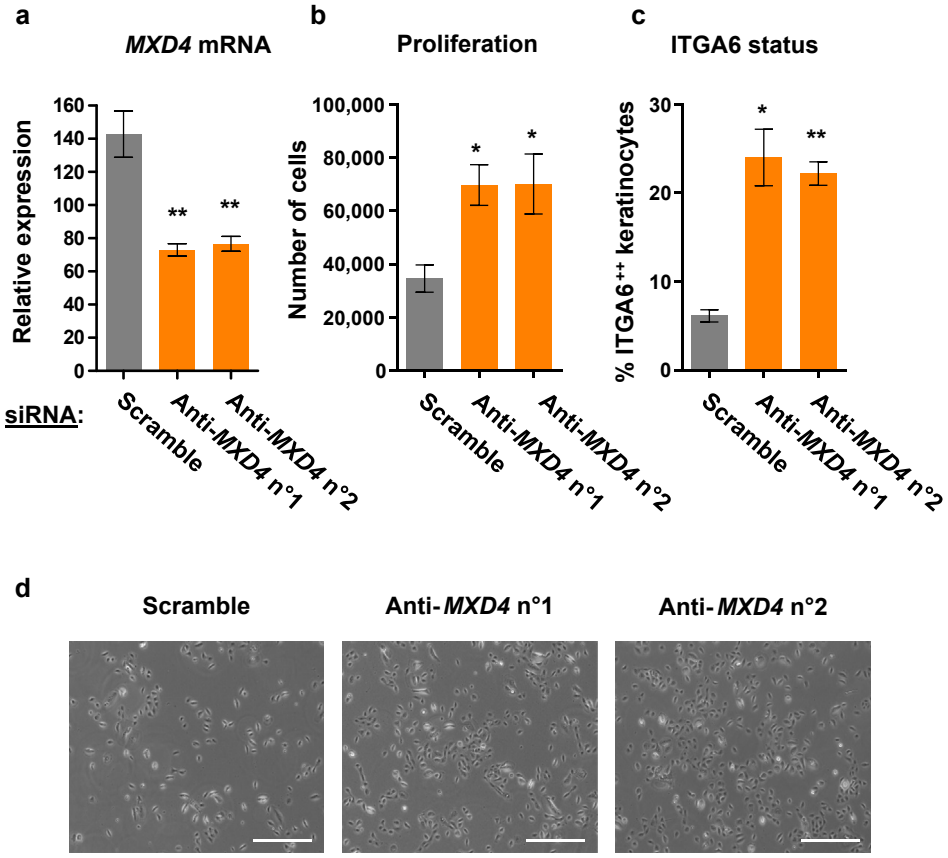

Supplementary Figure S8. Effects of siRNA-mediated repression of *MXD4*. Transient siRNA transfection (two different siRNA sequences and a scramble siRNA) (Supplementary Table S2) of keratinocytes was performed. (a) qRT-PCR of *MXD4* mRNA after siRNA transfection. Signals were normalized versus 18S transcript signal and scramble-transfected control cells (mean ± SEM, n = 9 biologically independent samples). (b) Keratinocytes grown in six-well plates were counted after 5 days of culture after transfection (mean ± SEM, n = 3 biologically independent samples). (c) ITGA6 expression in siRNA-transfected cells. Data represent the percentages of $ITGA6^{++}$ keratinocytes detected in each condition (mean ± SEM, n = 6 biologically independent samples). (d) Typical bright-field photographs of siRNA-treated keratinocyte cultures. Bars = 200 μm. $*P < 0.05$ and $**P < 0.01$. siRNA, small interfering RNA.

Supplementary Figure S9. Characteristics of the two lentiviral vectors used for shRNA-based *MXD4* repression. Vectors were designed by Vectalys SA. Two anti-*MXD4* siRNA sequences were selected in the human *MXD4* coding sequence (accession number CCDS3361) using a siRNA selection pipeline that takes into account thermodynamic properties and mRNA secondary structure data in addition to classical siRNA selection criteria. The selected siRNA sequences were then adapted to be used as an shRNA-mir: a loop of a human miRNA was added to generate a short hairpin, and a mismatch was created on the sense sequence to mimic the natural miRNA. Anti-*MXD4* sh1RNA vector: results are shown in the core manuscript. Anti-*MXD4* sh2RNA vector: results are shown in the Supplementary Materials and Methods. miRNA, microRNA; shRNA, short hairpin RNA; siRNA, small interfering RNA.

Knock down vector (GFP + anti-*MXD4* sh1RNA)

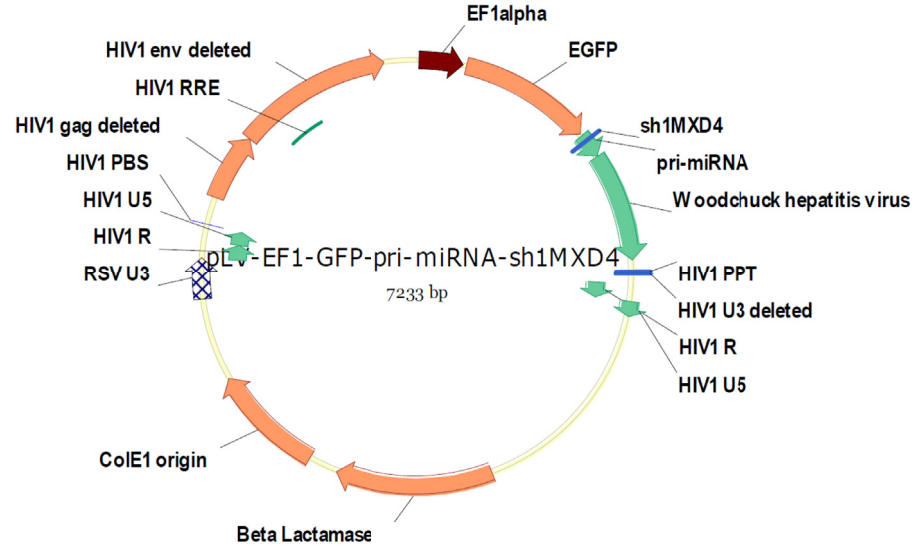

5′ CTAGCCAAGGTGAACATCAAGAATTTAATGTCTATACAATTCTTGATGTGCACCTTGG 3′
3′ GGTTCCACTTGTAGTTCTTAAATTACAGATATGTTAAGAACTACACGTGGAACCGATC 5′

miRNA loop
introduced mismatch

Knock down vector (GFP + anti-*MXD4* sh2RNA)

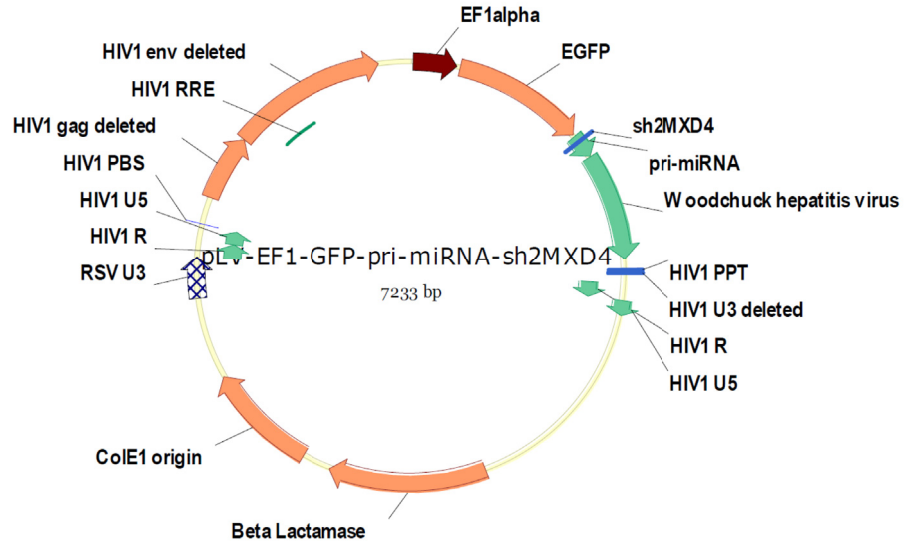

5′CTAGTCGCCAGGTAGAAAACAAATTTAATGTCTATACAATTTGTTTTCTCCCTGGCGA 3′
3′ AGCGGTCCATCTTTTGTTTAAATTACAGATATGTTAAACAAAAGAGGGACCGCTGATC 5′

miRNA loop
introduced mismatch

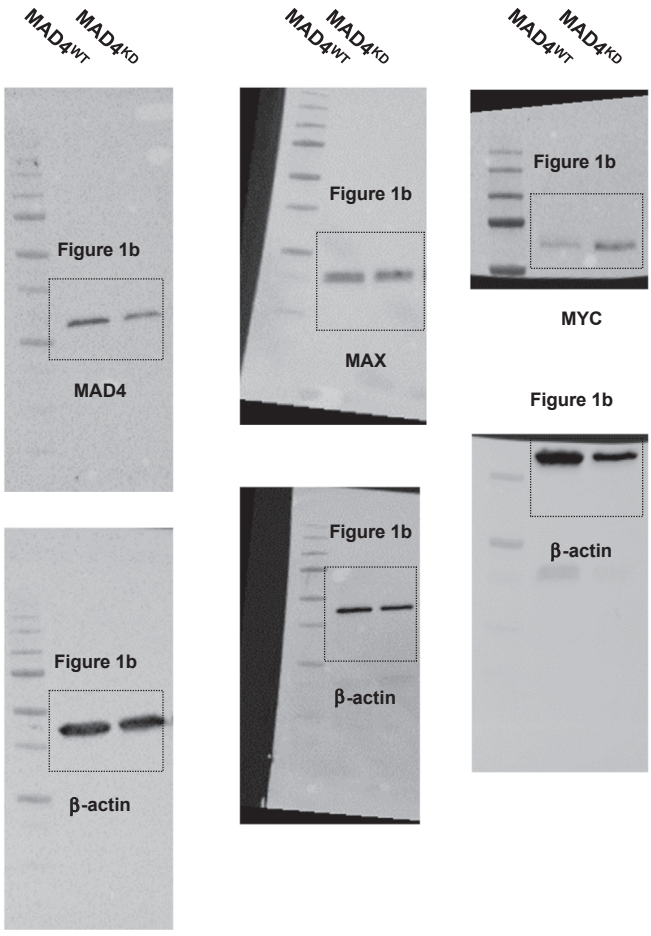

Supplementary Figure S10. Western blots. This figure corresponds to Figure 1. KD, knockdown; WT, wild-type.

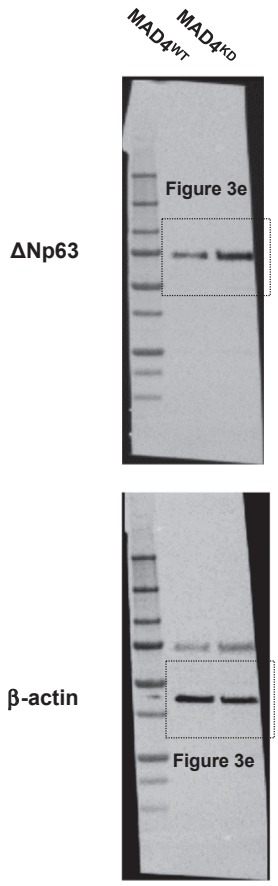

Supplementary Figure S11. Western blots. This figure corresponds to Figure 3. KD, knockdown; WT, wild-type.

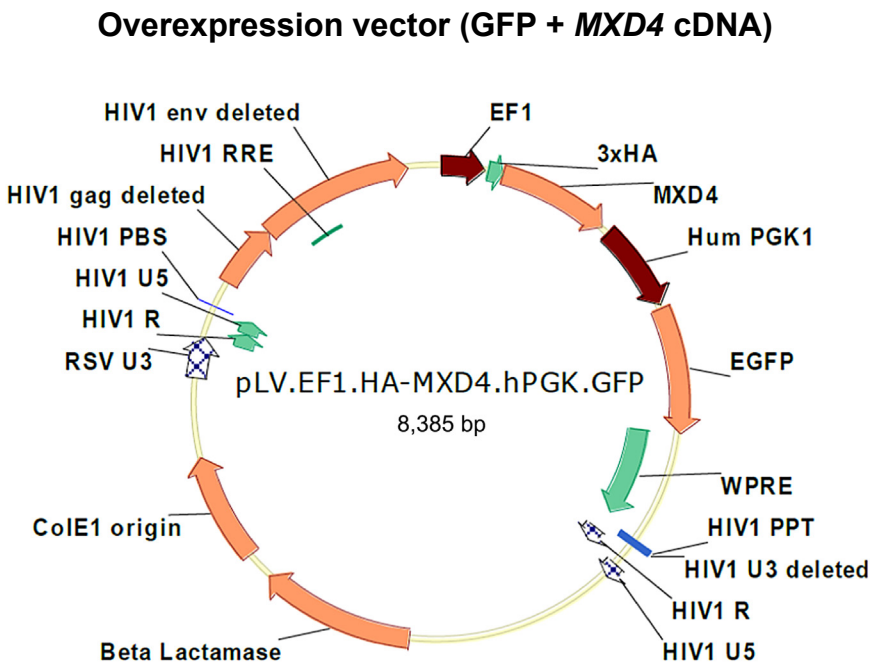

Supplementary Figure S12. Characteristics of the lentiviral vector used for *MXD4* cDNA overexpression. Vector was designed by Vectalys SA. Human *MXD4* coding sequence: accession number CCDS3361.